# 5B.9 A STATISTICAL EVALUATION OF THE SMPRF RANGE-VELOCITY MITIGATION TECHNIQUE

Evan Ruzanski
Colorado State University, Fort Collins, Colorado

John C. Hubbert*
University Center for Atmospheric Research, Boulder, Colorado

V. Chandrasekar
Colorado State University, Fort Collins, Colorado

Gregory Meymaris
University Center for Atmospheric Research, Boulder, Colorado

## 1. INTRODUCTION

The Simultaneous Multiple Pulse Repetition Frequency (SMPRF) algorithm is a radar pulsing scheme developed by J. Pirttila, M. Lehtinen, et. al. (1999; 2005) whose purpose in weather radar applications is to alleviate the effects of range/velocity ambiguity, also known as the range/Doppler dilemma.

The development of the SMPRF algorithm is explained and illustrated with mathematical examples (Pirtilla et al. 2005; Lehtinen 1999). The performance of the algorithm is then demonstrated by recovering a mean power and mean velocity profile calculated using actual weather signals. The results are presented graphically.

In this study, the performance of the SMPRF algorithm used for mean power recovery is analyzed in a more rigorous manner and limitations of such are recognized. After describing the background of the problem and operation of the SMPRF algorithm, simulation of an example code presented in (Pirtilla et al. 2005) for 4 power profiles is performed. The effects of the main factors affecting performance of the SMPRF algorithm are examined. These factors relate to the variability between inversion variables and power level separation of such. The report is concluded with a summary of results and observations with a discussion of such.

This study also introduces and investigates the methodology for estimating mean velocity using a spectral maxima technique used in the SMPRF algorithm.

## 2. DESCRIPTION OF THE SMPRF ALGORITHM

The SMPRF algorithm is an extension of the staggered PRT algorithm (Zrnic and Mahapatra 1985) in the sense an arbitrary number of pulses sent at different PRTs is used opposed to the two pulses used in the staggered PRT algorithm. In the SMPRF algorithm, the code is comprised of multiple pulses that are sent at different PRTs. This sequence is repeated to generate overlaid time series from which moment estimates are recovered.

To illustrate the operation of the SMPRF code, consider the example illustrative code given in (Pirtilla et al. 2005). This code is comprised of 4 PRTs: 750μs, 1200μs, 1500μs, and 1050μs. To simplify notation and make the example more tractable, it is noted that the greatest common denominator between each PRT in the set of PRTs comprising the code is $\Delta t = 150\mu s$. Each PRT can then be described as a multiple of this basic time unit. In this way, it is said the code consists of PRTs of 5, 8, 10, and 7 time units. This code is annotated as the "$SMPRF_{(150);\ 5,\ 8,\ 10,\ 7}$" code.

As will be shown later, the SMPRF algorithm can be written in matrix notation. The effect of choosing a larger $\Delta t$ increases the spacing of the subset of resolution volumes that are used in the inversion process in the SMPRF algorithm. This translates to fewer variables to recover in the inversion process but the spacing of the actual radar samples remains the same as dictated by the pulse width. The trade-off is that more repetitions of the inversion process must

* EOL/NCAR, Boulder, Colorado 80307, email: hubbert@ucar.edu

be performed. If sampling in weather radar is normally performed at $\Delta t = 1\mu s$, the inversion process will need to be performed $K = 150$ times for $\Delta t = 150\mu s$. This separation of the main inversion problem into $K$ mutually independent smaller inversion problems is not necessary as one large matrix dealing with more ranges can be inverted. For example, for a range resolution of 150 m, the inversion matrix will have *450 km/150 m = 3000* columns. The inversion of this larger matrix is less efficient and thus more computationally complex. The computational savings of this reduction are described in (Lehtinen 1999).

For the purposes of this study, the samples and ranges are restricted to integer multiples of $\Delta t$. This serves the purpose of clarity in explanation and illustration for the performance of the mean power recovery of the SMPRF algorithm.

Figure 1 illustrates the operation of the $\text{SMPRF}_{(150);\ 5,\ 8,\ 10,\ 7}$ code.

To illustrate the operation of the code, the return at time 31 is studied, as labeled in Figure 1. Pulses are transmitted according to the given code at times 0, 5, 13, 23, and 30 and repeated at times 35, 43, 53, 60, etc. for the number of blocks chosen to be transmitted. The number of transmitted blocks corresponds to the dwell time for measurements and translates to the length of the return time series at each measurement volume. In this study, the number of transmitted code blocks, i.e. the length of each time series for each measurement volume, is represented by *M.*

Reception of weather returns begins at time 31. This received complex value will have contributions from the previous pulses sent at times 30, 23 and 13. If it is desired to cover cloud tops up to 18 km, at the lowest elevation angle of $0.5^{o}$ and taking into account the curvature of the earth, the maximum measurement range of the radar is approximately 450 km. Since the maximum limiting range for weather returns is 450 km, any contribution from returns beyond 20 time units is disregarded, as,

$$r_{max} = 450\ km = \frac{cT_s}{2} = \frac{cN\Delta t}{2} \Rightarrow$$
$$N = \frac{900 \times 10^3}{3 \times 10^8 (150 \times 10^{-6})} = 20 \quad (1)$$

The time series of measurements collected at times 31, 61, 91, etc., $V_{31}$, will be comprised of the illumination of the 1st resolution volume corresponding to the pulse transmitted at times 30, 60, 90, etc., the 8th resolution volume corresponding to the pulse transmitted at times 23, 53, 83, etc., and the 18th resolution volume corresponding to the pulse transmitted at times 13, 43, 73, etc. The curved arrows in Figure 1 depict this relationship of pulses comprising the overlaid return time series.

The equations describing the measured returns $V_n;\ n \in \{31,\ 32,...,\ 60\}$ are constructed. This set of returns for the $\text{SMPRF}_{(150);\ 5,\ 8,\ 10,\ 7}$ code is shown in Equation 2. The time indices representing individual samples of each length-$M$ return time series, $\beta$, are omitted for convenience.

There will be no reception when the radar is transmitting, i.e., at times 35, 43, 53, 60, etc.

## 3. MOMENT CALCULATIONS USING THE SMPRF ALGORITHM

The following section outlines the procedure for estimation of the mean power and velocity from the received time series described by Equation 2.

### 3.1 MEAN POWER CALCULATION

The mean power is estimated for the $i^{th}$ volume from the measured time series corresponding to the $j^{th}$ PRT as shown,

$$\tilde{P}_i = \frac{1}{M}\sum_{k=1}^{M}\left|\beta_i^{(j)}(k)\right|^2 \quad (3)$$
$$j \in \{5,\ 13,\ 23,\ 30\},\ i \in \{1,2,...,20\}$$

The measured overlaid estimated power, $\tilde{Z}_{31}$ corresponding to $V_{31}$ can be written,

$$\tilde{Z}_{31} = \frac{1}{M}\sum_{k=1}^{M}\left|\tilde{V}_{31}\right|^2 = \frac{1}{M}\sum_{k=1}^{M}\left|\beta_1^{(30)}(k) + \beta_8^{(23)}(k) + \beta_{18}^{(13)}(k)\right|^2 \quad (4)$$

As a consequence of the independence between measurement volumes, Equation 4 can be written as shown in Equation 5 shown on the next page.

The equations for the measured overlaid estimated powers, $\tilde{Z}_n;\ n \in \{31,\ 32,...,\ 60\}$ can be written in matrix notation as shown in Equation 6.

$$
\begin{aligned}
V_{31} &= \beta_1^{(30)} + \beta_8^{(23)} + \beta_{18}^{(13)} & V_{46} &= \beta_3^{(13)} + \beta_{11}^{(5)} + \beta_{16}^{(30)} \\
V_{32} &= \beta_2^{(30)} + \beta_9^{(23)} + \beta_{19}^{(13)} & V_{47} &= \beta_4^{(13)} + \beta_{12}^{(5)} + \beta_{17}^{(30)} \\
V_{33} &= \beta_3^{(30)} + \beta_{10}^{(23)} + \beta_{20}^{(13)} & V_{48} &= \beta_5^{(13)} + \beta_{13}^{(5)} + \beta_{18}^{(30)} \\
V_{34} &= \beta_4^{(30)} + \beta_{11}^{(23)} & V_{49} &= \beta_6^{(13)} + \beta_{14}^{(5)} + \beta_{19}^{(30)} \\
V_{35} &= \textit{No data} & V_{50} &= \beta_7^{(13)} + \beta_{15}^{(5)} + \beta_{20}^{(30)} \\
V_{36} &= \beta_1^{(5)} + \beta_6^{(30)} + \beta_{13}^{(23)} & V_{51} &= \beta_8^{(13)} + \beta_{16}^{(5)} \\
V_{37} &= \beta_2^{(5)} + \beta_7^{(30)} + \beta_{14}^{(23)} & V_{52} &= \beta_9^{(13)} + \beta_{17}^{(5)} \\
V_{38} &= \beta_3^{(5)} + \beta_8^{(30)} + \beta_{15}^{(23)} & V_{53} &= \textit{No data} \\
V_{39} &= \beta_4^{(5)} + \beta_9^{(30)} + \beta_{16}^{(23)} & V_{54} &= \beta_1^{(23)} + \beta_{11}^{(13)} + \beta_{19}^{(5)} \\
V_{40} &= \beta_5^{(5)} + \beta_{10}^{(30)} + \beta_{17}^{(23)} & V_{55} &= \beta_2^{(23)} + \beta_{12}^{(13)} + \beta_{20}^{(5)} \\
V_{41} &= \beta_6^{(5)} + \beta_{11}^{(30)} + \beta_{18}^{(23)} & V_{56} &= \beta_3^{(23)} + \beta_{13}^{(13)} \\
V_{42} &= \beta_7^{(5)} + \beta_{12}^{(30)} + \beta_{19}^{(23)} & V_{57} &= \beta_4^{(23)} + \beta_{14}^{(13)} \\
V_{43} &= \textit{No data} & V_{58} &= \beta_5^{(23)} + \beta_{15}^{(13)} \\
V_{44} &= \beta_1^{(13)} + \beta_9^{(5)} + \beta_{14}^{(30)} & V_{59} &= \beta_6^{(23)} + \beta_{16}^{(13)} \\
V_{45} &= \beta_2^{(13)} + \beta_{10}^{(5)} + \beta_{15}^{(30)} & V_{60} &= \textit{No data}
\end{aligned}
\tag{2}
$$

$$
\tilde{Z}_{31} = \frac{1}{M}\sum_{k=1}^{M}\left|\beta_1^{(30)}(k)\right|^2 + \frac{1}{M}\sum_{k=1}^{M}\left|\beta_8^{(23)}(k)\right|^2 + \frac{1}{M}\sum_{k=1}^{M}\left|\beta_{18}^{(13)}(k)\right|^2 = \tilde{P}_1 + \tilde{P}_8 + \tilde{P}_{18} \tag{5}
$$

$$
\begin{bmatrix}
\tilde{Z}_{31} \\ \tilde{Z}_{32} \\ \tilde{Z}_{33} \\ \tilde{Z}_{34} \\ \tilde{Z}_{35} \\ \tilde{Z}_{36} \\ \tilde{Z}_{37} \\ \tilde{Z}_{38} \\ \tilde{Z}_{39} \\ \tilde{Z}_{40} \\ \tilde{Z}_{41} \\ \tilde{Z}_{42} \\ \tilde{Z}_{43} \\ \tilde{Z}_{44} \\ \tilde{Z}_{45} \\ \tilde{Z}_{46} \\ \tilde{Z}_{47} \\ \tilde{Z}_{48} \\ \tilde{Z}_{49} \\ \tilde{Z}_{50} \\ \tilde{Z}_{51} \\ \tilde{Z}_{52} \\ \tilde{Z}_{53} \\ \tilde{Z}_{54} \\ \tilde{Z}_{55} \\ \tilde{Z}_{56} \\ \tilde{Z}_{57} \\ \tilde{Z}_{58} \\ \tilde{Z}_{59} \\ \tilde{Z}_{60}
\end{bmatrix}
=
\begin{bmatrix}
1\,0\,0\,0\,0\,0\,0\,1\,0\,0\,0\,0\,0\,0\,0\,0\,0\,1\,0\,0 \\
0\,1\,0\,0\,0\,0\,0\,0\,1\,0\,0\,0\,0\,0\,0\,0\,0\,0\,1\,0 \\
0\,0\,1\,0\,0\,0\,0\,0\,0\,1\,0\,0\,0\,0\,0\,0\,0\,0\,0\,1 \\
0\,0\,0\,1\,0\,0\,0\,0\,0\,0\,1\,0\,0\,0\,0\,0\,0\,0\,0\,0 \\
0\,0\,0\,0\,0\,0\,0\,0\,0\,0\,0\,0\,0\,0\,0\,0\,0\,0\,0\,0 \\
1\,0\,0\,0\,0\,1\,0\,0\,0\,0\,0\,0\,1\,0\,0\,0\,0\,0\,0\,0 \\
0\,1\,0\,0\,0\,0\,1\,0\,0\,0\,0\,0\,0\,1\,0\,0\,0\,0\,0\,0 \\
0\,0\,1\,0\,0\,0\,0\,1\,0\,0\,0\,0\,0\,0\,1\,0\,0\,0\,0\,0 \\
0\,0\,0\,1\,0\,0\,0\,0\,1\,0\,0\,0\,0\,0\,0\,1\,0\,0\,0\,0 \\
0\,0\,0\,0\,1\,0\,0\,0\,0\,1\,0\,0\,0\,0\,0\,0\,1\,0\,0\,0 \\
0\,0\,0\,0\,0\,1\,0\,0\,0\,0\,1\,0\,0\,0\,0\,0\,0\,1\,0\,0 \\
0\,0\,0\,0\,0\,0\,1\,0\,0\,0\,0\,1\,0\,0\,0\,0\,0\,0\,1\,0 \\
0\,0\,0\,0\,0\,0\,0\,0\,0\,0\,0\,0\,0\,0\,0\,0\,0\,0\,0\,0 \\
1\,0\,0\,0\,0\,0\,0\,0\,1\,0\,0\,0\,0\,1\,0\,0\,0\,0\,0\,0 \\
0\,1\,0\,0\,0\,0\,0\,0\,0\,1\,0\,0\,0\,0\,1\,0\,0\,0\,0\,0 \\
0\,0\,1\,0\,0\,0\,0\,0\,0\,0\,1\,0\,0\,0\,0\,1\,0\,0\,0\,0 \\
0\,0\,0\,1\,0\,0\,0\,0\,0\,0\,0\,1\,0\,0\,0\,0\,1\,0\,0\,0 \\
0\,0\,0\,0\,1\,0\,0\,0\,0\,0\,0\,0\,1\,0\,0\,0\,0\,1\,0\,0 \\
0\,0\,0\,0\,0\,1\,0\,0\,0\,0\,0\,0\,0\,1\,0\,0\,0\,0\,1\,0 \\
0\,0\,0\,0\,0\,0\,1\,0\,0\,0\,0\,0\,0\,0\,1\,0\,0\,0\,0\,1 \\
0\,0\,0\,0\,0\,0\,0\,1\,0\,0\,0\,0\,0\,0\,0\,1\,0\,0\,0\,0 \\
0\,0\,0\,0\,0\,0\,0\,0\,1\,0\,0\,0\,0\,0\,0\,0\,1\,0\,0\,0 \\
0\,0\,0\,0\,0\,0\,0\,0\,0\,0\,0\,0\,0\,0\,0\,0\,0\,0\,0\,0 \\
1\,0\,0\,0\,0\,0\,0\,0\,0\,1\,0\,0\,0\,0\,0\,0\,0\,1\,0\,0 \\
0\,1\,0\,0\,0\,0\,0\,0\,0\,0\,1\,0\,0\,0\,0\,0\,0\,0\,1\,0 \\
0\,0\,1\,0\,0\,0\,0\,0\,0\,0\,0\,1\,0\,0\,0\,0\,0\,0\,0\,1 \\
0\,0\,0\,1\,0\,0\,0\,0\,0\,0\,0\,0\,1\,0\,0\,0\,0\,0\,0\,0 \\
0\,0\,0\,0\,1\,0\,0\,0\,0\,0\,0\,0\,0\,1\,0\,0\,0\,0\,0\,0 \\
0\,0\,0\,0\,0\,1\,0\,0\,0\,0\,0\,0\,0\,0\,1\,0\,0\,0\,0\,0 \\
0\,0\,0\,0\,0\,0\,0\,0\,0\,0\,0\,0\,0\,0\,0\,0\,0\,0\,0\,0
\end{bmatrix}
\begin{bmatrix}
\tilde{P}_1 \\ \tilde{P}_2 \\ \tilde{P}_3 \\ \tilde{P}_4 \\ \tilde{P}_5 \\ \tilde{P}_6 \\ \tilde{P}_7 \\ \tilde{P}_8 \\ \tilde{P}_9 \\ \tilde{P}_{10} \\ \tilde{P}_{11} \\ \tilde{P}_{12} \\ \tilde{P}_{13} \\ \tilde{P}_{14} \\ \tilde{P}_{15} \\ \tilde{P}_{16} \\ \tilde{P}_{17} \\ \tilde{P}_{18} \\ \tilde{P}_{19} \\ \tilde{P}_{20}
\end{bmatrix}
\tag{6}
$$

Equation 6 can be written more succinctly as,

$$\underline{\tilde{Z}} = A\underline{\tilde{P}} \quad (7)$$

This study considers evaluation of the SMPRF algorithm under the condition of infinite SNR. In the presence of noise, an additive noise term would be included in the equation above.

The least squares solution to Equation 7 yields the mean power estimate and is given by (Lehtinen 1999),

$$\underline{\hat{P}} = \left(A^T A\right)^{-1} A^T Z = A^{+}\underline{\tilde{Z}} \quad (8)$$

In Equation 8, $A^{+}$ is the Moore-Penrose matrix inverse (Ben-Israel and Greville 1977)

### 3.2 MEAN VELOCITY CALCULATION

As shown in (Pirtilla et al. 2005) and following the steps in the derivation of the maximum unambiguous velocity for the staggered PRT algorithm described above (Zrnic and Mahapatra 1985), the maximum unambiguous velocity for the SMPRF algorithm is given by,

$$v_{MAX,SMPRF} = \pm\lambda /(4 * min(PRT_{i,SMPRF} - PRT_{j,SMPRF})); \quad (9)$$

$$i \neq j$$

Similar to the maximum unambiguous velocity for the staggered PRT algorithm, the maximum unambiguous velocity for the SMPRF algorithm is a function of the radar's wavelength and minimum time separation between the PRTs in the given code.

For the $SMPRF_{(150);\ 5,\ 8,\ 10,\ 7}$ code with $\Delta t$ = *150μs*, this yields,

$$v_{MAX,SMPRF} = \pm 0.0536 /(4 \times 150 \times 10^{-6}) = \quad (10)$$

$$\pm 89.33\ m/s$$

This value, which corresponds to a velocity of about 200 miles per hour, is adequate for the measurement of weather phenomena.

Whereas matrix inversion was used to recover average power estimates, when dealing with mean velocity recovery, the matrix inversion procedure is unnecessary if pulses in the code are not equal to integer multiples of other pulses within the code. This ensures no autocorrelation function (ACF) sample ambiguity (Pirtilla et al. 2005).

The mean velocity procedure is now explained. All overlaid return time series are correlated pairwise. Based on the property that measurements from different measurement volumes are independent, unevenly spaced samples of the ACF plus a noise term are generated. A high-resolution power spectrum is computed from these ACF samples using statistical inversion techniques. The peak of this spectrum is taken to be the mean velocity estimate.

The block diagram for the SMPRF mean velocity recovery procedure is shown in Figure 2.

The correlation is shown to be,

$$\tilde{R}_i[n] = \frac{1}{M}\sum_{k=1}^{M}\left(V_{\tau_1}(k)V^{*}_{\tau_2}(k)\right) - \eta; \quad (11)$$

$$\tau_1, \tau_2 \in \{31, ..., 60\}, \forall\, \tau_1 \neq \tau_2$$

Where,

$$V_{\{\tau_1,\tau_2\}} = \sum_m \beta^{(j)}_{i'_{\{\tau_1,\tau_2\}}}; \quad (12)$$

$$i'_{\{\tau_1,\tau_2\}} \in \{1,...,20\},$$

$$j \in \{30,23,13,5\}$$

$$m = \sum_{h=1}^{20} A_{\{\tau_1,\tau_2\},h} \quad (13)$$

$$n = |\tau_1 - \tau_2| \quad (14)$$

$$i = i' \ \forall\ i'_{\tau_1} = i'_{\tau_2} \quad (15)$$

$$\eta \sim N(0,\sigma_n^2) \quad (16)$$

To illustrate this, consider this procedure illustrated for the returns from measurements volumes 31 and 36,

$$V_{31} = \beta_1 + \beta_8 + \beta_{18} \quad (17)$$

$$V_{36} = \beta_1 + \beta_6 + \beta_{13} \quad (18)$$

$$E\left[V_{31}V_{36}\right] = R_1[5] + \eta \quad (19)$$

All returns without contributions from common volumes will be independent and such ACF lag values are set to zero. It is believed that the noise generated by this process will be the limiting factor for the mean velocity recovery process. As will be illustrated later in this report, the variance of the noise term in the equations above depends upon the amount of overlaid power.

Using the example $SMPRF_{(150);\ 5,\ 8,\ 10,\ 7}$ code, the complete set of ACF lag values is shown in Table 1,

| Volume (*i*) | Lag values (*n*) |
|---|---|
| 1 | 5, 8, 10, 13, 18, 23 |
| 2 | 5, 8, 10, 13, 18, 23 |
| 3 | 5, 8, 10, 13, 18, 23 |
| 4 | 5, 8, 10, 13, 18, 23 |
| 5 | 8, 10, 18 |
| 6 | 5, 8, 10, 13, 18, 23 |
| 7 | 5, 8, 13 |
| 8 | 7, 13, 20 |
| 9 | 5, 7, 8, 12, 13, 20 |
| 10 | 5, 7, 12 |
| 11 | 5, 7, 8, 12, 13, 20 |
| 12 | 5, 8, 13 |
| 13 | 8, 12, 20 |
| 14 | 5, 7, 8, 12, 13, 20 |
| 15 | 5, 7, 8, 12, 13, 20 |
| 16 | 5, 7, 8, 12, 13, 20 |
| 17 | 5, 7, 12 |
| 18 | 7, 10, 17 |
| 19 | 5, 7, 8, 12, 13, 20 |
| 20 | 5, 17, 22 |

Table 1. *ACF lag values computed using* $SMPRF_{(150);5,\ 8,\ 10,\ 7}$ *code.*

It is shown in Table 1 that different ranges will have both different number and different values of the ACF lags. In general, there will be $n(n-1)/2 + 1$ ACF samples, $n(n-1)$ from the pairwise correlations and $1$ from the mean power estimate. The lack of ability to receive while transmitting accounts for the lower number of recovered ACF lags in certain volumes.

The calculation of the spectrum from the unevenly spaced ACF values for each measurement volume is performed as follows. The Discrete Fourier Transform (DFT) is applied to each measurement volume ACF sample vector producing the sample power spectrum, as shown,

$$\tilde{S}_i[k] = \sum_{n=0}^{N-1} \tilde{R}_i(n) e^{-\frac{2\pi j}{N} nk} \; ; k = 0, \ldots, N-1 \qquad (20)$$

The number of points used in the DFT calculation is chosen freely, with the resulting zero padding producing linear interpolation in the frequency domain (Roberts and Mullis 1987).

The location of the peak of the resulting sample power spectrum translated to the velocity domain is taken to be the mean velocity estimate.

## 4. SIMULATION RESULTS OF MEAN POWER RECOVERY USING THE SMPRF ALGORITHM

Four power profiles are simulated and recovered using the SMPRF algorithm: a flat 10 dB range profile, a triangular range profile with 50 dB power level separation, a triangular range profile with 15 dB power level separation, and a range profile consisting of one range gate with a signal level of 20 dB and the rest set to –100 dB. The results are compared to those for a uniform PRT scheme using the same power profiles.

The maximum unambiguous range of the uniform PRT scheme is set to 450 km and the maximum unambiguous velocity will be,

$$v_{MAX,UNIFORM} = \pm\lambda / (4 * PRT)) = \pm 0.0536 / (0.012) = \pm 4.47 \ m/s \qquad (21)$$

The uniform PRT value used for comparison to the SMPRF results will be equal to the *N* value for the SMPRF code, i.e., *20 time units = 3000μs*.

For all power profile recovery simulations, one polarization channel of the dual-polarization radar simulation technique described in (Chandrasekar et al. 1986) is simulated. The mean velocity is randomized between +/- $v_a$ and spectrum width of 4 m/s is selected, which is at the center of the range of spectrum width values simulated in (Sachidananda et al. 1998). The radar frequency is 5.6GHz ($\lambda = 5.36$ *cm*). Two hundred iterations are run for statistics. Fifteen blocks are used for the $SMPRF_{(150);\ 5,\ 8,\ 10,\ 7}$ code, which translates to a dwell time of 67.5ms. Length 22 time series are used for the uniform PRT schemes for comparison to both SMPRF codes translating to a dwell time of 66 ms. These are reasonable dwell times relative to those Volume Coverage Patterns (VCPs) used by NEXRAD (NEXRAD ROC 2006).

In the figures illustrating average power profile recovery, the red horizontal lines at each range gate represent the mean value of the average power estimates for that range gate calculated over the set of 200 iterations. The blue rectangle represents one standard deviation of the average power estimate at the corresponding range gate centered about the mean. The whiskers extending from this rectangle represent a width of 4 standard deviations centered about the mean, i.e. 2

standard deviation above and 2 standard deviations below the mean. It should be noted that for a normal distribution, approximately 95% of the data would lie within 2 standard deviations on either side of the mean. In the results presented below, since decibel scale is used, this will not be the case. Outlier values are denoted by the red "+"s.

The simulation results for the $SMPRF_{(150);\ 5,\ 8,\ 10,\ 7}$ code with maximum unambiguous measurement range of 450 km and corresponding uniform PRT scheme are seen in Figure 3 through Figure 10.

The results show that for a similar dwell time, the $SMPRF_{(150);\ 5,\ 8,\ 10,\ 7}$ code lends to recovered estimates which are biased if the power separation between range gates is approximately 15-20 dB and for any level of power separation, the variance of the recovered estimates is higher versus estimates recovered using a uniform PRT scheme. As will be shown later, the most likely reasons for this reduced number of samples used for the estimates for a given dwell time and the numerical imprecision associated with the variability of the parameters used in the inversion process.

### 4.2 ANALYSIS OF FACTORS AFFECTING MEAN POWER RECOVERY PERFORMANCE OF THE SMPRF ALGORITHM

There will inherently be variation in the power estimates for each range from each PRT that comprise the inversion variables. This effectively creates a condition where the inversion equation becomes underdetermined, i.e., instead of 20 variables to recover in the inversion process, there will now be 80.

The finite-length effects of the time series on the performance of the SMPRF algorithm are examined. It is well known that the variance for average power estimates will be higher for such parameters computed from shorter-length time series (Bringi and Chandrasekar 2001). To this effect, the recovery of the average power estimates of the 50 dB and flat 10 dB profiles as used previously are simulated using the $SMPRF_{(150);5,\ 8,\ 10,\ 7}$ code with a maximum unambiguous range of 450 km with 4000 repetitions, i.e., dwell time is equal to 18 seconds. The results are shown in Figure 11 and Figure 12, for the two profiles respectively.

Upon comparison of Figure 11 with Figure 5, it is apparent there is much less biasing and variance in the average power estimate at each range gate. Figure 5 shows the power separation before biasing occurs is about 15 dB. Figure 11 shows as the dwell time is increased and the mean power estimates improve, i.e., have lower variance, this separation is increased to about 25 dB.

Next, the $SMPRF_{(150);5,\ 8,\ 10,\ 7}$ with maximum unambiguous range of 450 km code is used to recover the 50 dB triangular profile to illustrate the effect of recovering average power estimates calculated from time series simulated with various spectrum widths. Figure 13 through Figure 15 show this effect with $\sigma_v = 8$ *m/s,* $\sigma_v = 1$ *m/s*, and $\sigma_v = 0$ *m/s* (deterministic), respectively.

Figure 13 through Figure 15 show that as $\sigma_v$ is reduced, there is more correlation between members of the received overlaid time series from which mean power estimates are calculated. This translates to less variability between variables in the inversion process. In the case of deterministic, i.e., $\sigma_v = 0$, signals, the accuracy of the recovery process is limited by the precision of the computer generating the estimates.

Next, the variance of the differences in average power estimates calculated from the received time series are explored. The time series are length $M = 30$, $\Delta t = 30*150\mu s = 4.5$ *ms*, with a power of 10 dB. The number of iterations run to generate the variance statistics is 50,000. The results are shown in Figure 16.

For a more rigorous analysis of the effects of the variability between average power estimates calculated from a given range volume, the following tables using the parameters from the $SMPRF_{(150);5,\ 8,\ 10,\ 7}$ code, i.e. 4 PRTs and $\Delta t = 150\mu s$ are presented, depicting,

$$V_\beta = 10\log_{10}\left[\frac{\left|\beta_1^i\right|^2}{\left|\beta_1^j\right|^2}\right]; \qquad (22)$$

$$i, j \in \{1,2,3,4\},\ i \neq j$$

A 1000-bin histogram of this difference (in dB) between the mean power calculated from time series collected from illuminations by the (arbitrarily chosen) first and second PRTs, i.e., PRTs pulsed at time 30, 60, 90, etc. and 5, 35, 65, etc., generated over 50,000 iterations is shown in Figure 17.

Table 2 and Table 3 show the mean and standard deviation for the difference in mean power estimates (in dB) for all pair differences across the 4 PRTs for $\sigma_v = 4$ *m/s* and $\sigma_v = 1$ *m/s.*

| μ | *j = 1* | *2* | *3* | *4* |
|---|---|---|---|---|
| *i = 1* | 0 | 0.0045 | 0.0414 | 0.0046 |
| *2* | -0.0045 | 0 | 0.0369 | 0.0001 |
| *3* | -0.0414 | -0.0369 | 0 | -0.0369 |
| *4* | -0.0046 | -0.0001 | 0.0369 | 0 |
| *σ* | *j = 1* | *2* | *3* | *4* |
| *i = 1* | 0 | 0.8682 | 1.1705 | 0.6889 |
| *2* | 0.8682 | 0 | 1.0186 | 0.9854 |
| *3* | 1.1705 | 1.0186 | 0 | 0.9578 |
| *4* | 0.6889 | 0.9854 | 0.9578 | 0 |

Table 2. *Mean and standard deviation of average power estimates between PRTs for first range gate in 50dB triangular profile, $\sigma_v$ = 4 m/s.*

| μ | *j = 1* | *2* | *3* | *4* |
|---|---|---|---|---|
| *i = 1* | 0 | -0.0021 | -0.0028 | 0.0005 |
| *2* | -0.0021 | 0 | -0.0007 | 0.0026 |
| *3* | -0.0028 | -0.0007 | 0 | 0.0033 |
| *4* | 0.0005 | 0.0026 | 0.0033 | 0 |
| *σ* | *j = 1* | *2* | *3* | *4* |
| *i = 1* | 0 | 0.0621 | 0.1353 | 0.1746 |
| *2* | 0.0621 | 0 | 0.0847 | 0.1331 |
| *3* | 0.1353 | 0.0847 | 0 | 0.0636 |
| *4* | 0.1746 | 0.1331 | 0.0636 | 0 |

Table 3. *Mean and standard deviation of average power estimates between PRTs for first range gate in 50dB triangular profile, $\sigma_v$ = 1 m/s.*

Table 2 and Table 3 show the differences in mean power estimates from similar range resolutions that cause variability in the inversion parameters. While the mean values of the differences are small for $\sigma_v$ = *1 m/s* and $\sigma_v$ = *4 m/s*, the standard deviation values are significant. This point along with the fact large power separation cause biasing in the mean power estimates are the main factors limiting the performance of the SMPRF algorithm for mean power recovery.

## 5. INVESTIGATION OF THE PERFORMANCE OF THE SPECTRAL MAXIMA TECHNIQUE USED IN THE SMPRF ALGORITHM TO RECOVER MEAN VELOCITY

The technique used in (Pirtilla et al. 2005) to estimate the mean velocity of the weather signal is noteworthy in its difference from the popular pulse pair technique. In this technique, the power spectrum is computed from the unevenly sampled ACF lag values using the Fast Fourier Transform (FFT) and the location of the peak of this spectrum, translated from the frequency domain to the velocity domain, is taken to be the estimate for the mean velocity.

The following simulations illustrate this technique in a fashion relative to the SMPRF algorithm. In Figure 18, the power spectrum ($N_{FFT}$ = *512*) of a simulated 64-point weather signal is shown, with $\sigma_v$ = *2 m/s*, *v = 30 m/s*, *P = 20 dB*, and *PRT = 150 μs*.

The peak location of the power spectrum shown in Figure 18 is located at bin $k_{max}$ = *175* which translated to the velocity estimate, *v '* by,

$$v' = v_a - \frac{2v_a k_{max}}{N_{FFT}} = 28.26 \ \frac{m}{s} \tag{23}$$

Where,

$$v_a = \frac{\lambda}{4PRT} = \frac{5.36 \times 10^{-2}}{4(150 \times 10^{-6})} = 89.33 \ \frac{m}{s} \tag{24}$$

The unevenly spaced samples of the ACF of the return weather signal calculated using the SMPRF algorithm can be modeled as the modulation of an evenly spaced ACF with spacing equal to the PRT by a binary masking sequence in which the positions of the ACF lag values estimated using the SMPRF algorithm are set to a value of "1" and the rest set to "0". This amounts to a convolution in the frequency domain of the two respective spectra.

This is illustrated using the unevenly spaced ACF of the first volume, $R_1[k]$, calculated using the $SMPRF_{(150);\ 5,\ 8,\ 10,\ 7}$ code shown in Equation 25.

In this example, the binary masking sequence, $M_1[k]$, is given by Equation 27.

The power spectrum of the binary masking sequence, $M_1[k]$, is shown in Figure 19.

The unevenly spaced ACF of the first measurement volume, $R_1[k]$, is then given by,

$$R_1[k] = M_1[k] \cdot X[k] \tag{29}$$

Where,

$X[k]$ is the original ACF of the weather signal.

The power spectrum of the return weather signal using the $SMPRF_{(150);\ 5,\ 8,\ 10,\ 7}$ code, $S_1(\omega)$, given as the Discrete Fourier Transform of $R_1[k]$, is shown in Figure 20.

In Figure 20,the peak of the spectra is located at $k_{max}$ = 174 corresponding to a velocity of *v' = 28.61 m/s*.

Several factors affect the performance of the spectral maxima technique to estimate mean velocity. These include the number of FFT points taken ($N_{FFT}$), spectrum width ($\sigma_v$) of the weather signal, signal-to-noise ratio (SNR) of the weather signal return, and structure of SMPRF code, i.e., structure of the binary mask. Each is investigated in further detail below.

$$R_1[k] = \{P_1\ 0\ 0\ 0\ 0\ R_1[5]\ 0\ 0\ R_1[8]\ 0\ R_1[10]\ 0\ 0\ R_1[13]\ 0\ 0\ 0\ 0\ R_1[18]\ 0\ 0\ 0\ 0\ R_1[23]\} \quad (25)$$

Where,

$P_1$ is the mean power estimate for the first measurement volume, and

$$R_1[-k] = R_1^*[k] \quad (26)$$

$$M_1[k] = \{1\ 0\ 0\ 0\ 0\ 1\ 0\ 0\ 1\ 0\ 1\ 0\ 0\ 1\ 0\ 0\ 0\ 0\ 1\ 0\ 0\ 0\ 0\ 1\} \quad (27)$$

Where,

$$M_1[-k] = M_1[k] \quad (28)$$

### 5.1 EFFECT OF $N_{FFT}$ ON THE PERFORMANCE OF THE SPECTRAL MAXIMA TECHNIQUE FOR MEAN VELOCITY RECOVERY

The number of FFT points used in calculation of the power spectrum from which the peak is determined to acquire the mean velocity estimate affects the resolution of the power spectrum, with a higher-resolution spectrum equating to a smoother spectrum. Figure 21 and Figure 22 illustrate the power spectra of weather signals recovered using the $SMPRF_{(150);\ 5,\ 8,\ 10,\ 7}$ code using $N_{FFT} = 64$ and $N_{FFT} = 4096$, respectively.

The mean error and standard deviation of the mean velocity estimate as a function of the number of FFT points used in the calculated power spectrum using the simulation parameters above is shown in Figure 23 and Figure 24.

The results presented in Figure 23 and Figure 24 show the best performance of the spectral maxima technique to estimate mean velocity is attained when using more points, however in the interest of saving computational power, the number of points can be as low as 1024 can be used with similar accuracy of the estimates.

### 5.2 EFFECT OF SPECTRUM WIDTH ON THE PERFORMANCE OF THE SPECTRAL MAXIMA TECHNIQUE FOR MEAN VELOCITY RECOVERY

The spectrum width of the weather signal plays a substantial role in the accuracy of the mean velocity estimates. For larger spectrum widths, the location of the peak value in the power spectrum will be adversely affected by overlap incurred during the frequency-domain convolution of the power spectrum of the return weather signal with that of the binary masking sequence. This point is illustrated in Figure 25 and Figure 26, which depict the power spectrums of recovered weather signals with spectrum widths of $\sigma_v = 1$ *m/s* and $\sigma_v = 8$ *m/s*, respectively, using the SMPRF algorithm.

Upon examination of Figure 25 and Figure 26, it is evident that mean velocity estimates of weather signals with larger spectrum widths will be less accurate due to the spreading of the respective power spectrum and the resulting alteration of the location of the spectral peak.

The mean error and standard deviation of the mean velocity estimate as a function of the spectrum width is shown in Figure 27 and Figure 28, where it is seen that the performance of this technique begins to deteriorate for spectral widths above 2 m/s.

### 5.3 EFFECT OF SNR ON THE PERFORMANCE OF THE SPECTRAL MAXIMA TECHNIQUE FOR MEAN VELOCITY RECOVERY

When the ACF lag values are computed using the SMPRF algorithm, correlation between different resolution volumes appears as noise. This creates an effective SNR dependent upon the amount of overlaid power in each received return signal.

To this point, all simulations were run using infinite SNR. Figure 29 and Figure 30 depict power spectra of weather signals recovered using the SMPRF algorithm with *SNR = 10 dB* and *SNR = -10 dB*, respectively.

The mean error and standard deviation of the mean velocity estimate as a function of the SNR is shown in Figure 31 and Figure 32, where it is seen that the performance begins to deteriorate for SNRs less than about 10 dB.

### 5.4 EFFECT OF SMPRF CODE SELECTION ON THE PERFORMANCE OF THE SPECTRAL MAXIMA TECHNIQUE FOR MEAN VELOCITY RECOVERY

The choice of code will influence the number and position of ACF lag estimates used to recover the mean velocity of the received weather signal.

The mean power estimate is a component in the ACF used to recover the mean velocity estimate and was shown to have considerable error and variance when power separations between resolution volumes at greater than about 15 dB. The power spectrum is computed and shown without the mean power estimate in Figure 33.

The spectrum for a weather signal recovered using only ACF lags 0, 5 and 8 is shown in Figure 34.

The mean error and standard deviation of mean velocity estimates using various lag values in the computation is shown in Table 4.

| ***Lag values used in estimate*** | ***μ (m/s)*** | ***σ (m/s)*** |
|---|---|---|
| *23, 18, 13, 10, 8, 5* | 0.39 | 1.37 |
| *18, 13, 10, 8, 5, 0* | 0.30 | 1.23 |
| *13, 10, 8, 5, 0* | 0.40 | 1.08 |
| *10, 8, 5, 0* | 0.36 | 1.03 |
| *8, 5, 0* | 0.45 | 2.44 |
| *5, 0* | 36.0 | 51.0 |

Table 4. *Performance comparison of mean velocity estimates using various lag values in computation.*

## 6. CONCLUSIONS

There is a trade-off inherent to the SMPRF algorithm in that as the maximum unambiguous range and velocity values are increased, more overlays are present in a given coding scheme that creates larger variance and bias in the mean power estimate. It was shown using the example code given in (Pirtilla et al. 2005) that the SMPRF algorithm provides reasonable recovery of mean power up to range overlay separations up to about 15 dB. This power separation is largely affected by the structure of the inversion matrix $A$, i.e., the number of ones in each row of $A$.

The SMPRF code structure choices influence the greatest common denominator between the pulses, i.e., $\Delta t$, which is a factor in determining the maximum unambiguous velocity of the code. According to the equation describing the maximum unambiguous velocity, it is beneficial in this sense to have two pulses in the code separated by one time unit to yield the highest possible maximum unambiguous velocity for a given code.

The mean velocity estimation using the SMPRF code is accomplished by correlating range-overlaid return signals, taking the spectrum of the resulting unevenly spaced ACF, and translating the location of the peak in the frequency domain to a mean velocity estimate. It was shown that this spectral maxima technique is noisier than the standard pulse pair technique when used on uniform PRT weather return time series and is adversely affected by factors such as using less than 512-point FFTs, spectrum widths above about 2 m/s, SNR lower than about 10 dB, and an SMPRF code choice yielding less than 3 ACF lags used to estimate the mean velocity.

In general, the range/Doppler dilemma still exists for the SMPRF algorithm but in a different sense than that for the uniform PRT scheme. In the uniform PRT scheme, the range/Doppler dilemma resulted in range/velocity folding and thus ambiguity of range and/or velocity estimates. In the case of the SMPRF scheme, this ambiguity is exhibited in decreased quality of the recovered moment estimates.

**Acknowledgement.** This work was supported by Vaisala, Inc., under UCAR grant #B08134.

## 7. REFERENCES

Ben-Israel, A. and T. Greville, 1977: *Generalized Inverses: Theory and Applications.* Wiley, 384 pp.

Bringi, V.N., and V. Chandrasekar. 2001: *Polarimetric Doppler Weather Radar: Principles and Applications.* Cambridge Press, 636 pp.

Chandrasekar, V., and Coauthors, 1986: Statistical properties of dual-polarized radar signals. Preprints, *23rd Conf. on Radar Meteorology,* Snowmass, CO, Amer. Meteor. Soc., 193-196.

Lehtinen, M. S., 1999: Method and System for Measuring Radar Reflectivity and Doppler Shift by Means of a Pulse Radar, World Intellectual Property Organization International Patent Publication Number WO 99/49332.

NEXRAD Radar Operations Center, WSR-88D: 2006; [online] http://www.roc.noaa.gov/

Pirtilla, J., and Coauthors, 2005: A Proposed Solution to the Range-Doppler Dilemma of Weather Radar Measurements by Using the SMPRF Codes, Practical Results, and a Comparison with Operational Measurements, *J. Appl. Meteor.,* **44**: 1375-1390.

Roberts, R., and C. Mullis, 1987: *Digital Signal Processing,* Addison-Wesley, 578 pp.

Sachidananda, M., and Coauthors, 1998: Signal Design and Processing Techniques for WSR-88D Ambiguity Resolution, National Severe Storms Laboratory Report, Part 2.

Zrnic, D. S., and P. Mahapatra, 1985: Two methods of ambiguity resolution in pulsed Doppler weather radars, *IEEE Trans. Aerosp. Elect. Syst.*, **4**: 470-483.

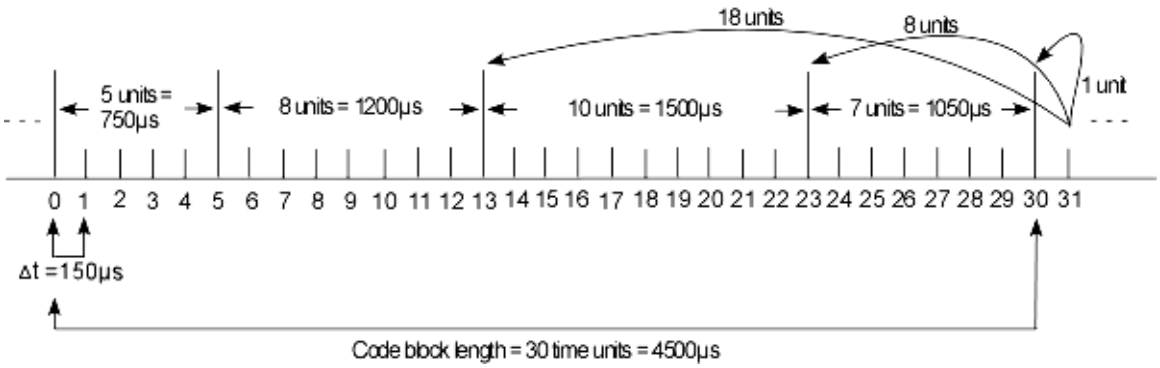


Figure 1. *Illustration and operation of the SMPRF code; 5, 8, 10, 7 PRTs, Δt = 150μs.*


Figure 2. *Block diagram of SMPRF mean velocity recovery procedure.*

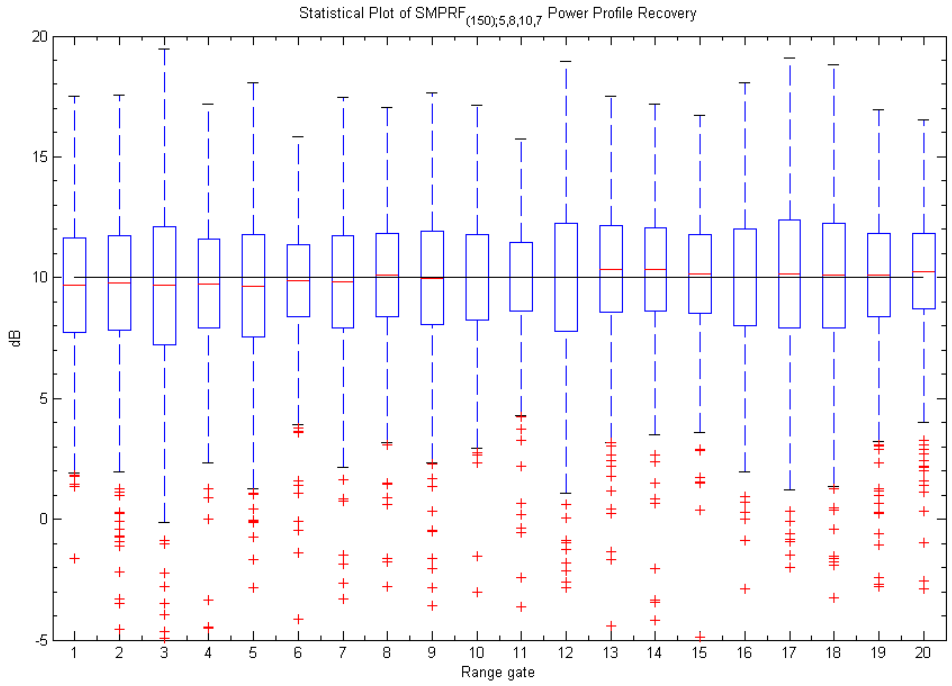


Figure 3. *Power profile recovery for 10 dB flat profile, SMPRF$_{(150);\ 5,\ 8,\ 10,\ 7}$ code.*

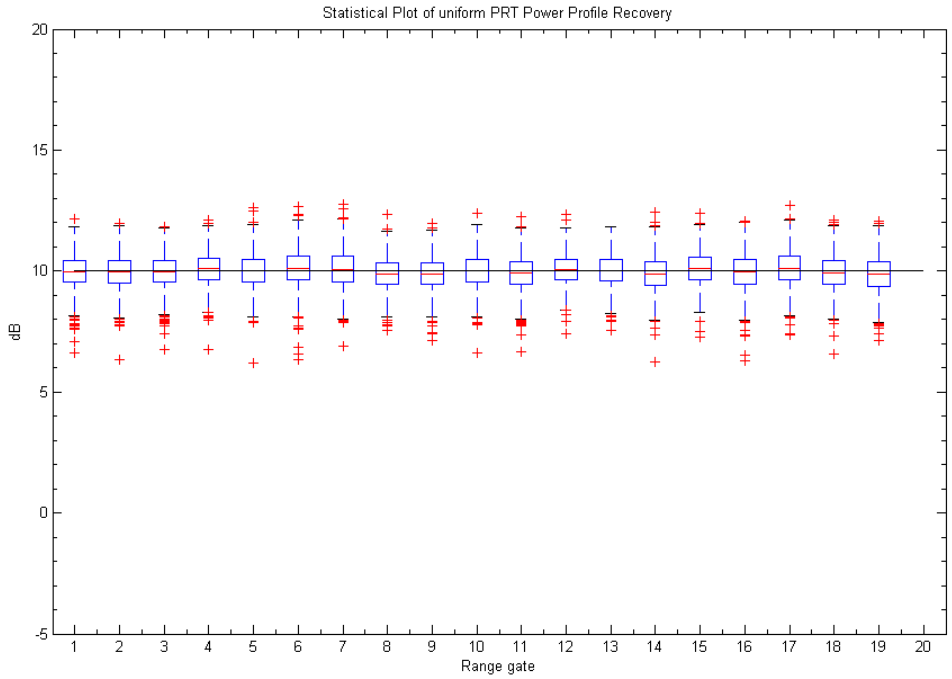


Figure 4. *Power profile recovery for 10 dB flat profile, uniform PRT.*

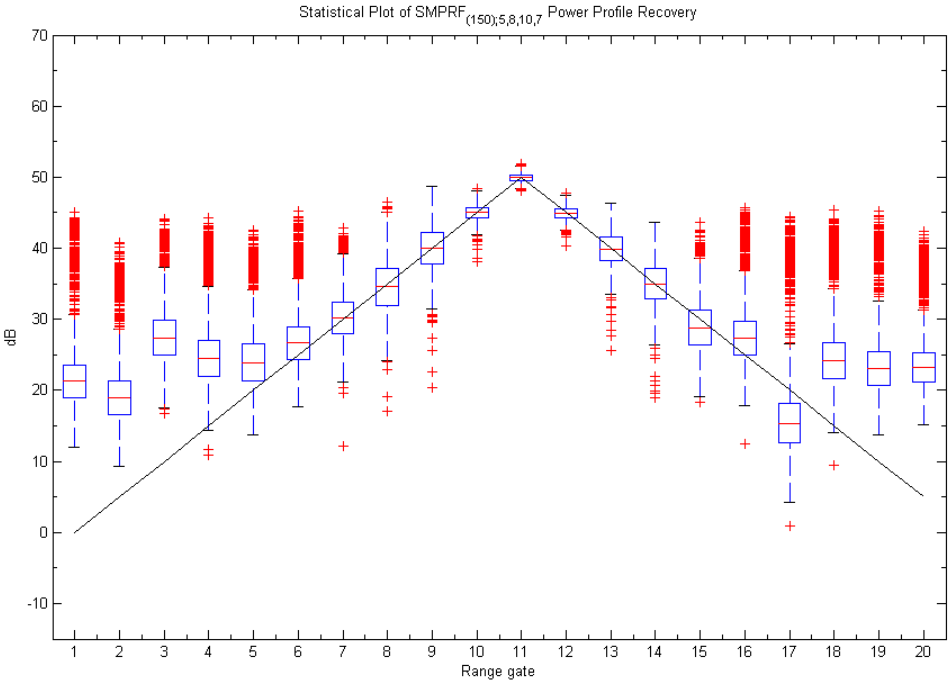


Figure 5. *Power profile recovery for 50 dB triangular profile, SMPRF$_{(150);\ 5,\ 8,\ 10,\ 7}$ code.*

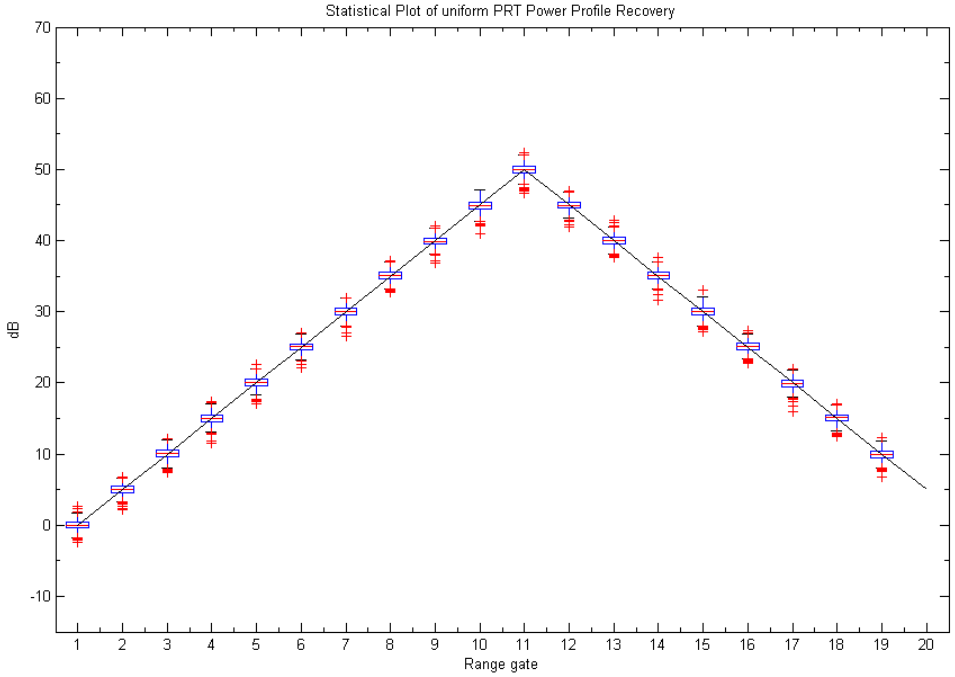


Figure 6. *Power profile recovery for 50 dB triangular profile, uniform PRT.*

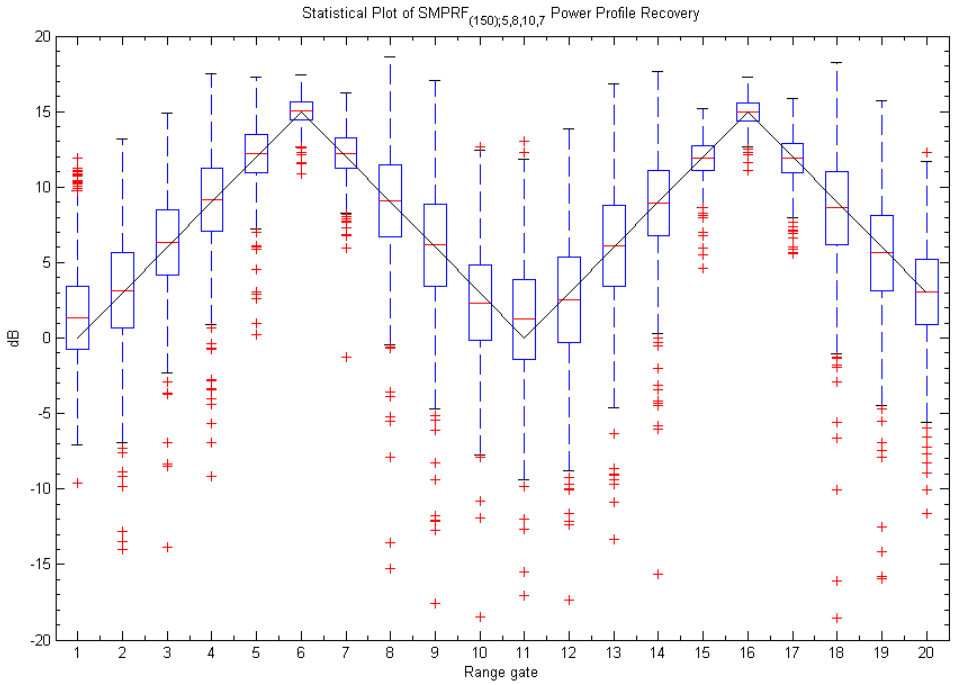


Figure 7. *Power profile recovery for 15 dB triangular profile, SMPRF$_{(150);\ 5,\ 8,\ 10,\ 7}$ code.*

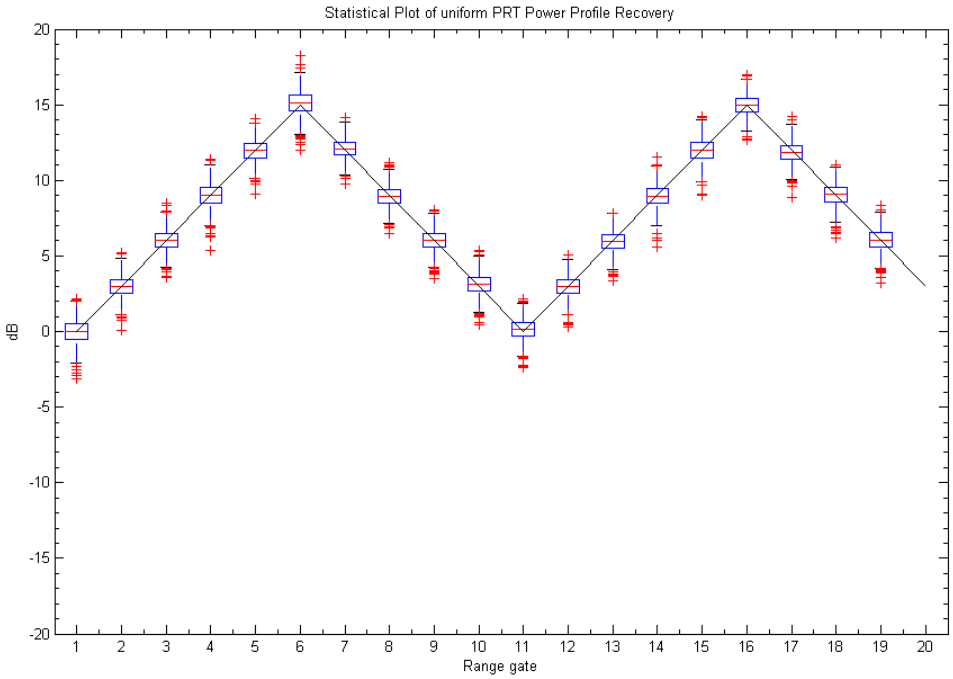


Figure 8. *Power profile recovery for 15 dB triangular profile, uniform PRT.*

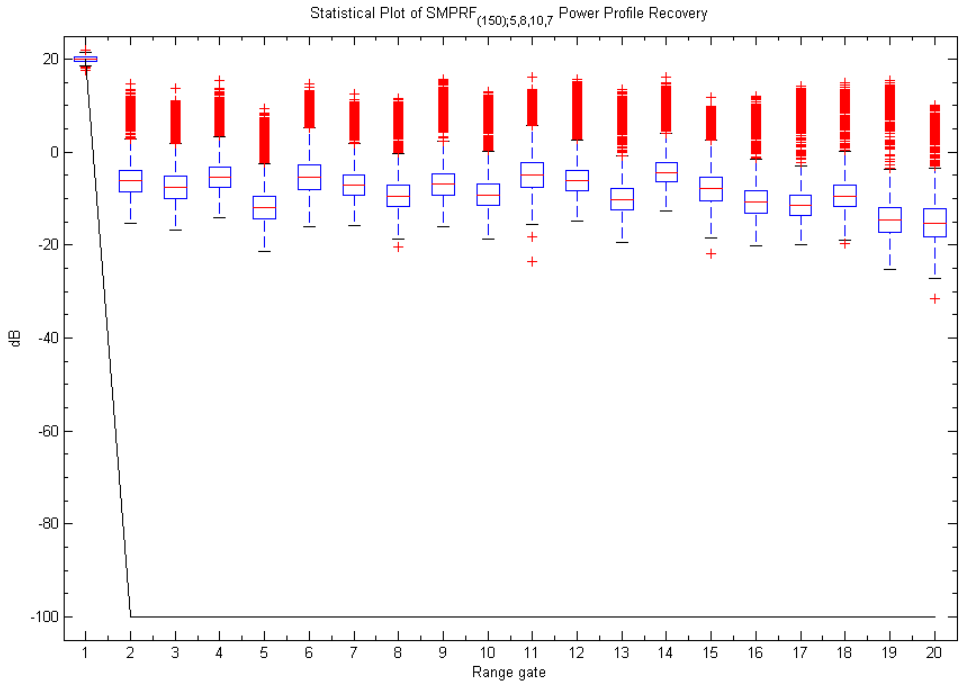


Figure 9. *Power profile recovery for 20 dB single-gate profile, SMPRF$_{(150);\ 5,\ 8,\ 10,\ 7}$ code.*

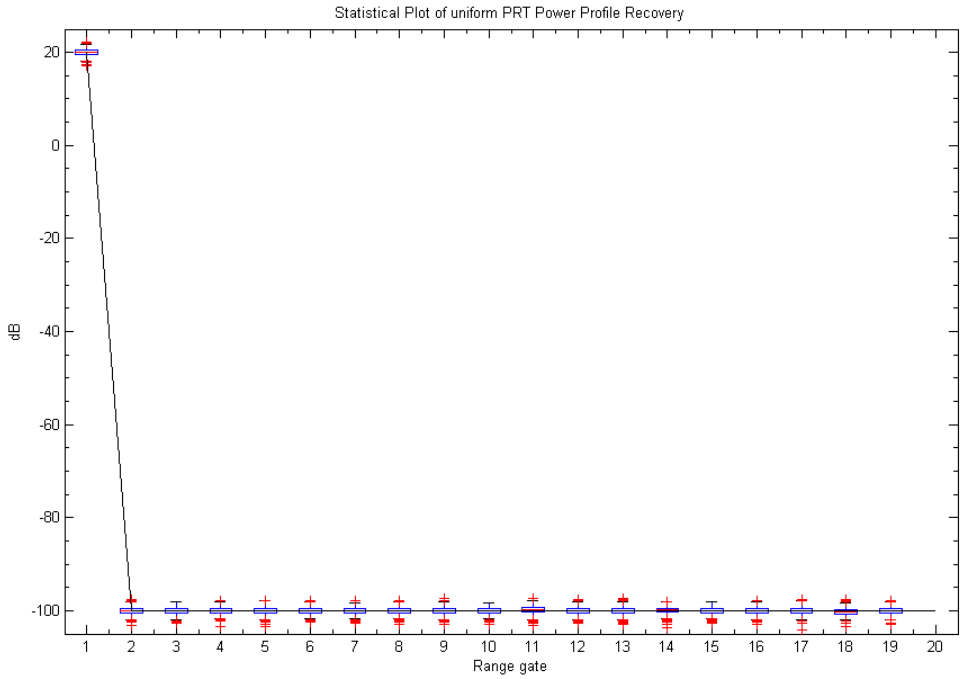


Figure 10. *Power profile recovery for 20 dB single-gate profile, uniform PRT.*

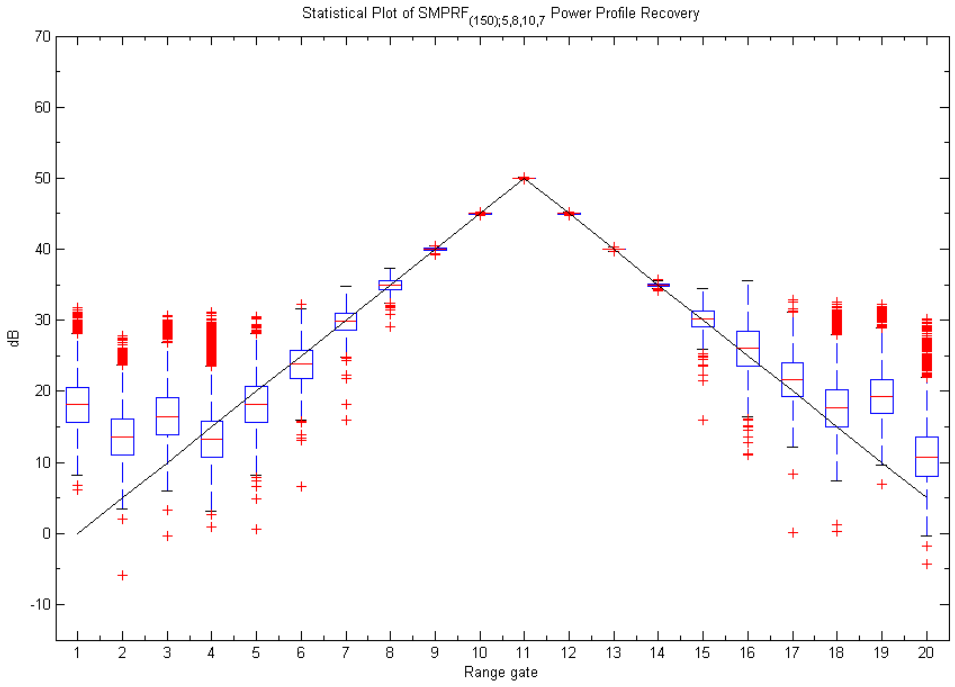


Figure 11. *Power profile recovery for 50 dB triangular profile, $SMPRF_{(150);\ 5,\ 8,\ 10,\ 7}$ with maximum unambiguous range of 450 km, 4000 blocks used for simulation.*

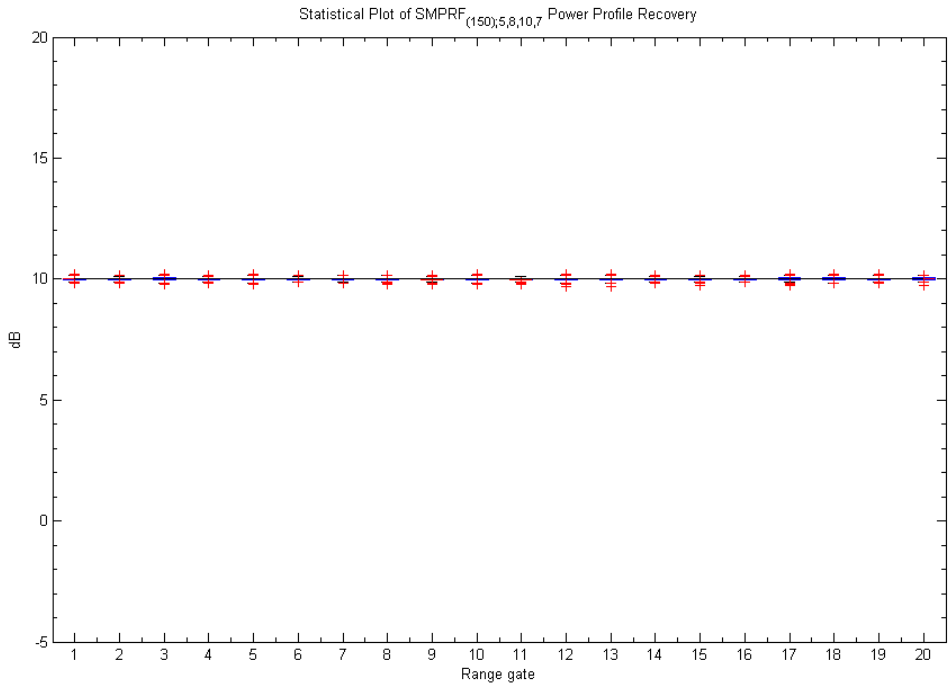


Figure 12. *Power profile recovery for 10 dB flat profile, $SMPRF_{(150);\ 5,\ 8,\ 10,\ 7}$ with maximum unambiguous range of 450 km, 4000 blocks used for simulation.*

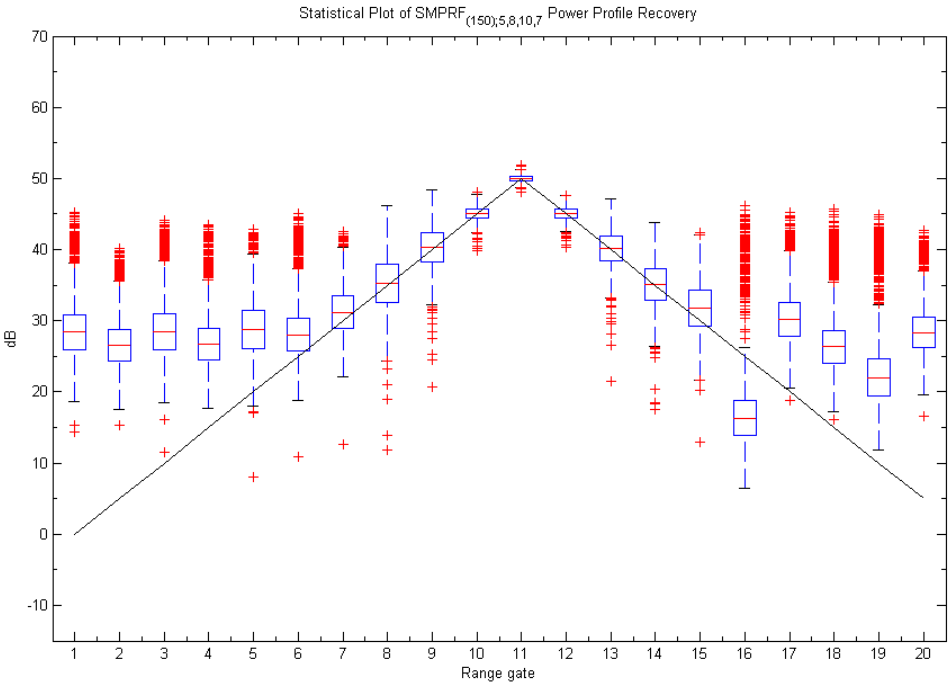


Figure 13. *Power profile recovery for 50 dB triangular profile, $SMPRF_{(150);\ 5,\ 8,\ 10,\ 7}$ with maximum unambiguous range of 450 km, $\sigma_v$ = 8 m/s.*

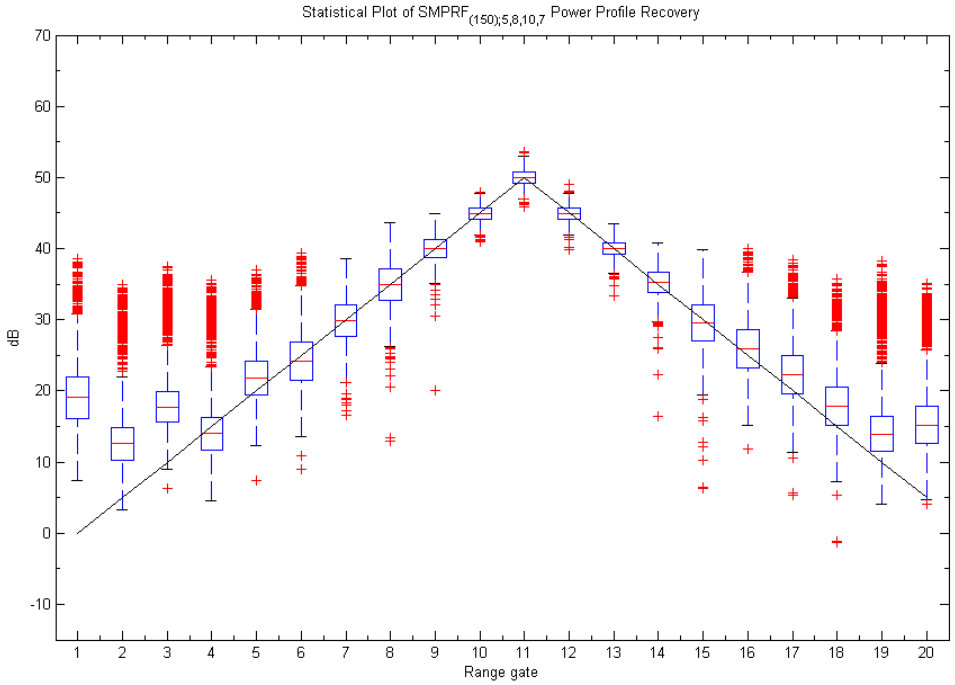


Figure 14. *Power profile recovery for 50 dB triangular profile, $SMPRF_{(150);\ 5,\ 8,\ 10,\ 7}$ with maximum unambiguous range of 450 km, $\sigma_v$ = 1 m/s.*

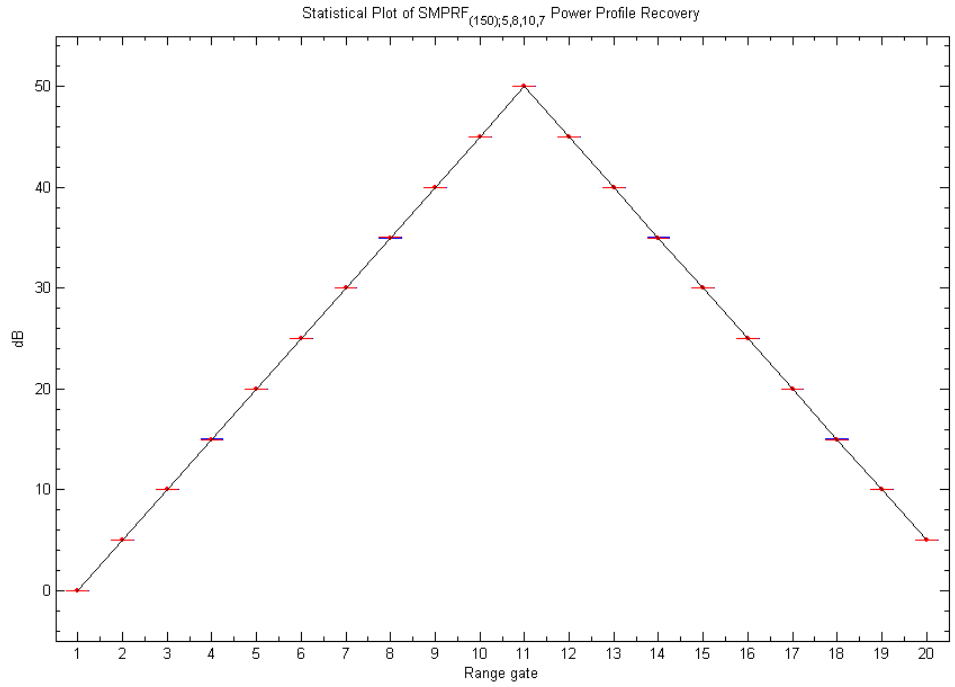


Figure 15. *Power profile recovery for 50 dB triangular profile, $SMPRF_{(150);\ 5,\ 8,\ 10,\ 7}$ with maximum unambiguous range of 450 km, $\sigma_v$ = 0 m/s (deterministic).*

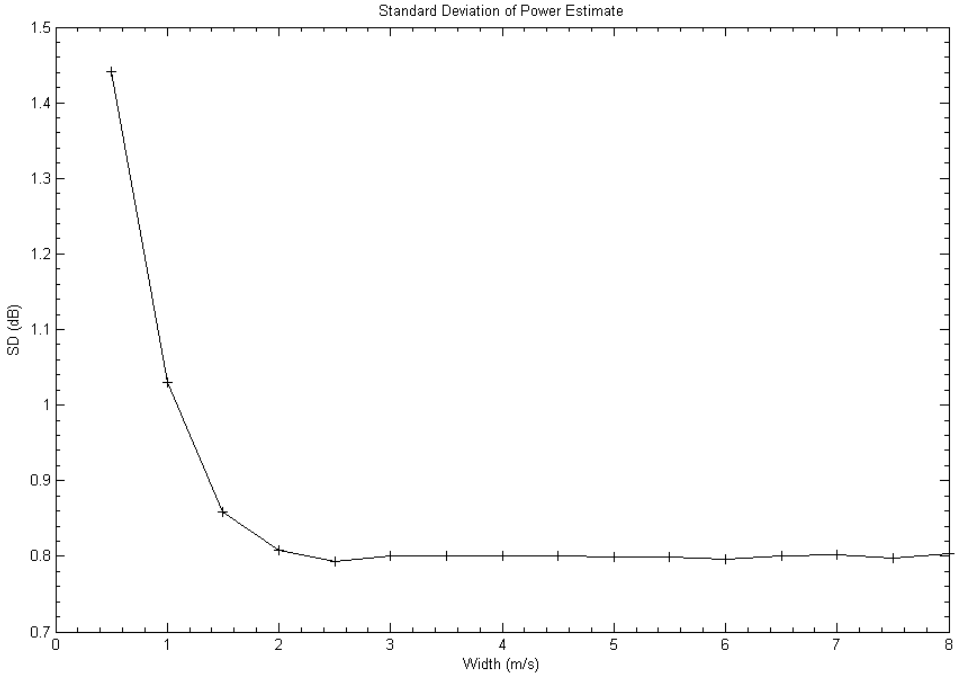


Figure 16. *Standard deviation of average power estimate vs. spectrum width.*

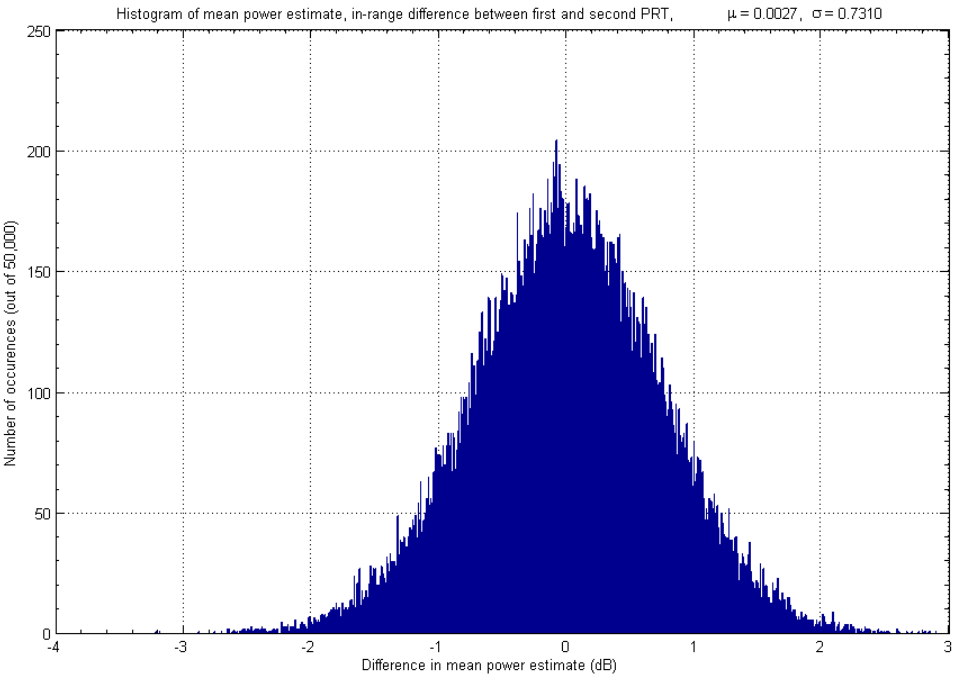


Figure 17. *Histogram of the difference of average power estimates for range gate one between the time series collected from illuminations by the first and second PRT.*

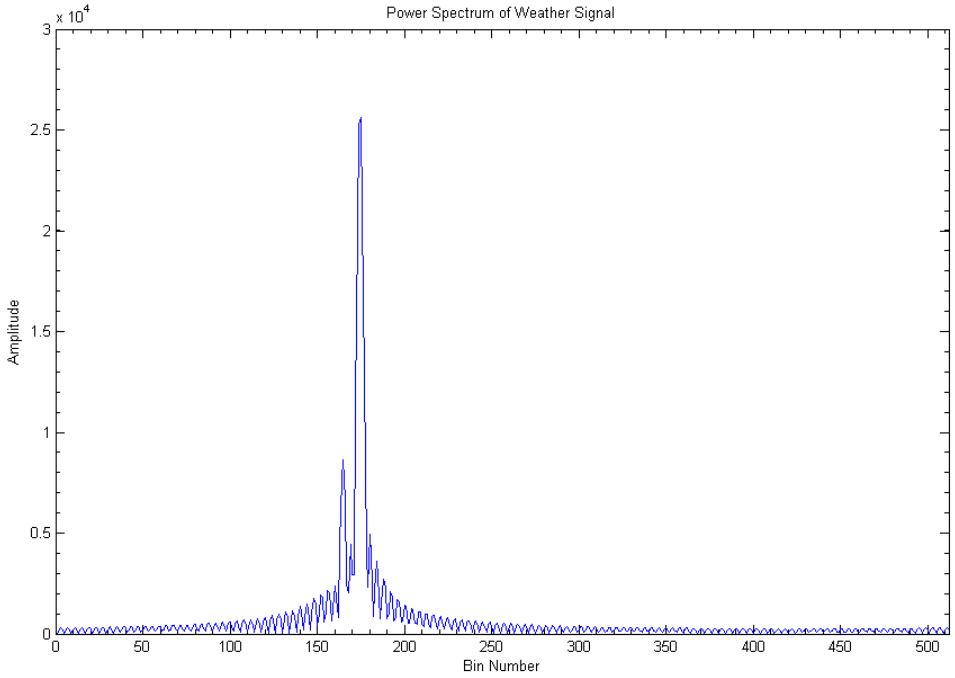


Figure 18. *Power spectrum of weather signal.*

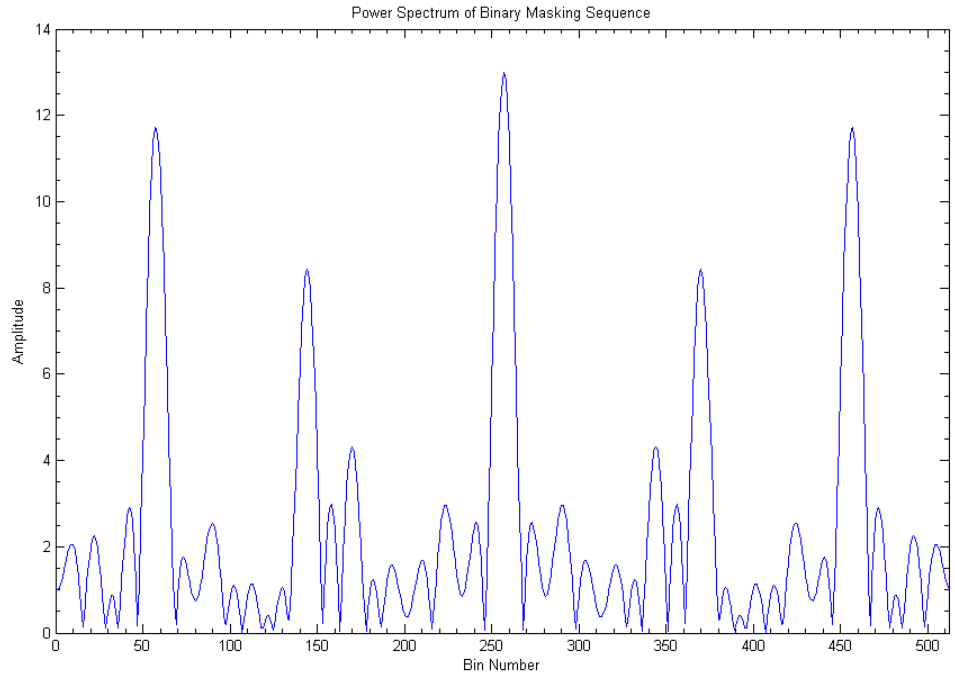


Figure 19. *Power spectrum of binary masking sequence.*

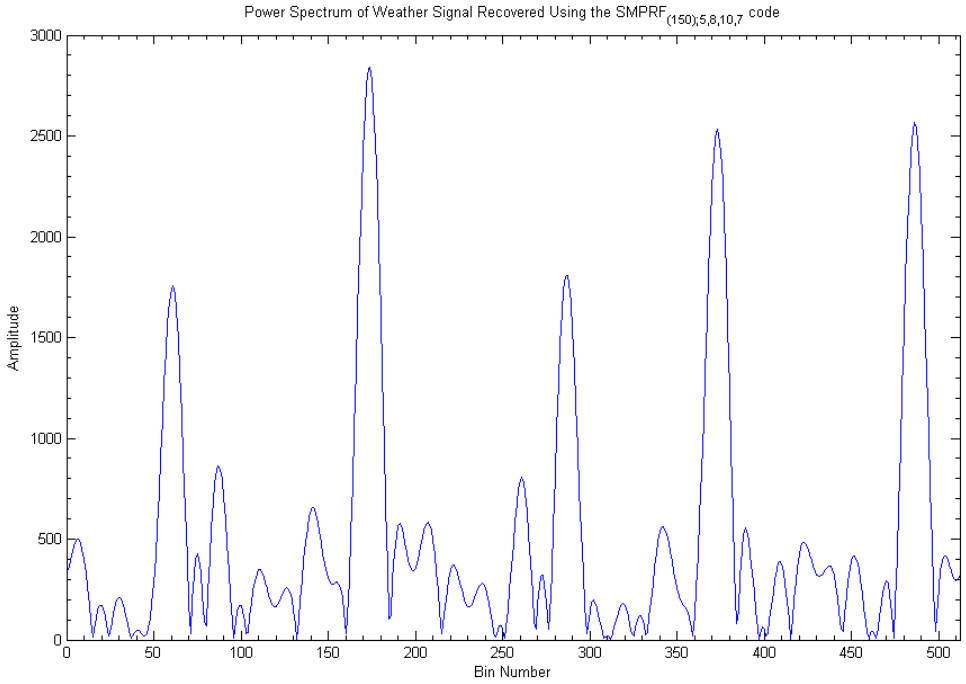


Figure 20. *Power spectrum of weather signal recovered using the SMPRF$_{(150);5,8,10,7}$ code.*

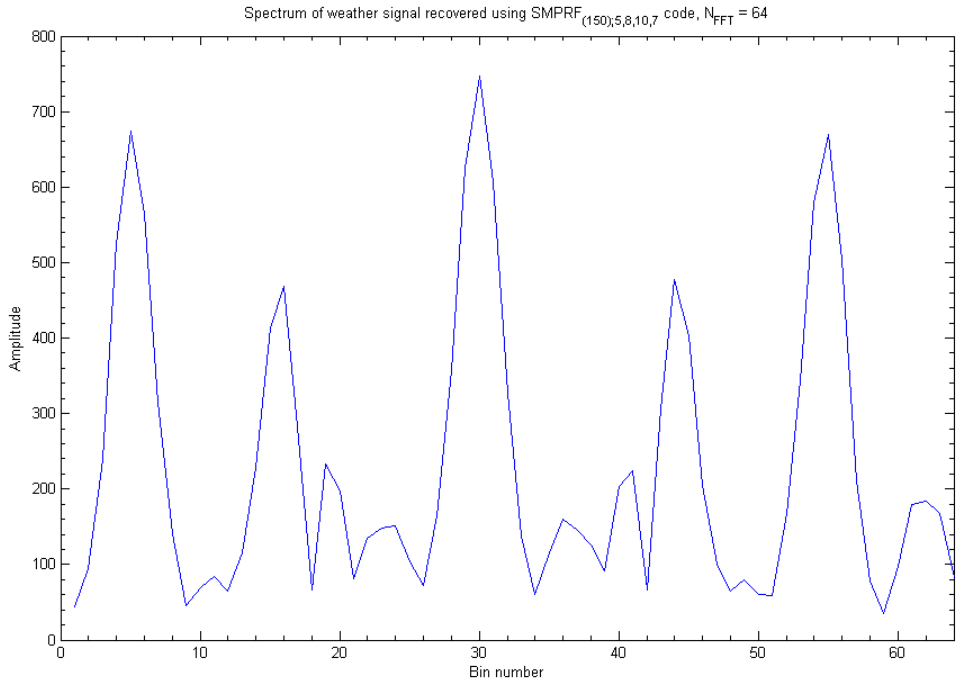


Figure 21. *Spectrum of weather signal recovered using SMPRF$_{(150);5, 8, 10, 7}$ code, $N_{FFT}$ = 64.*

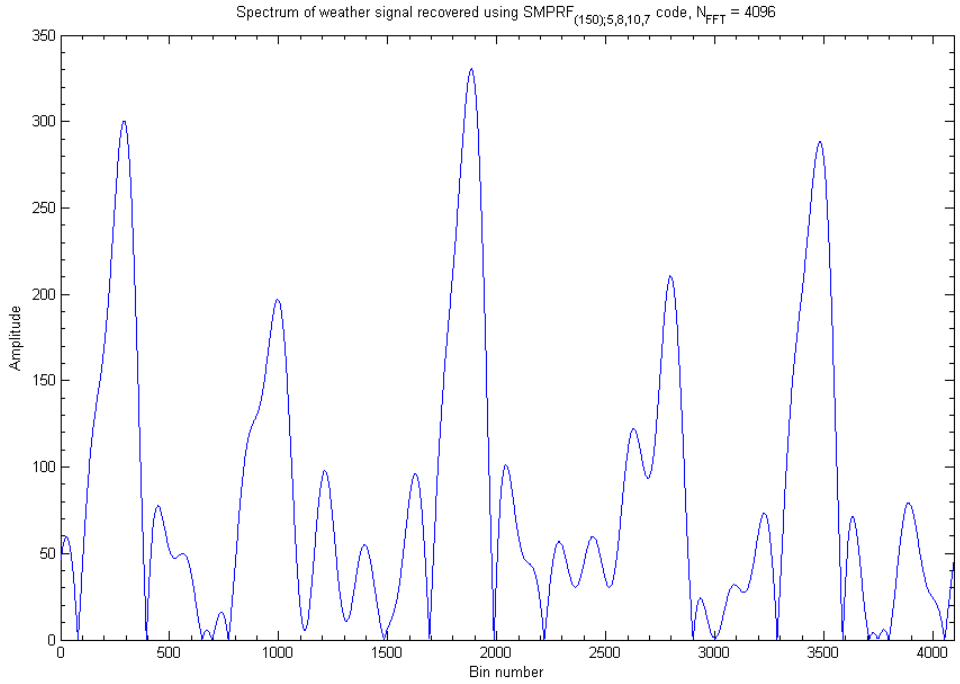


Figure 22. *Spectrum of weather signal recovered using SMPRF$_{(150);5,\ 8,\ 10,\ 7}$ code, $N_{FFT}$ = 4096.*

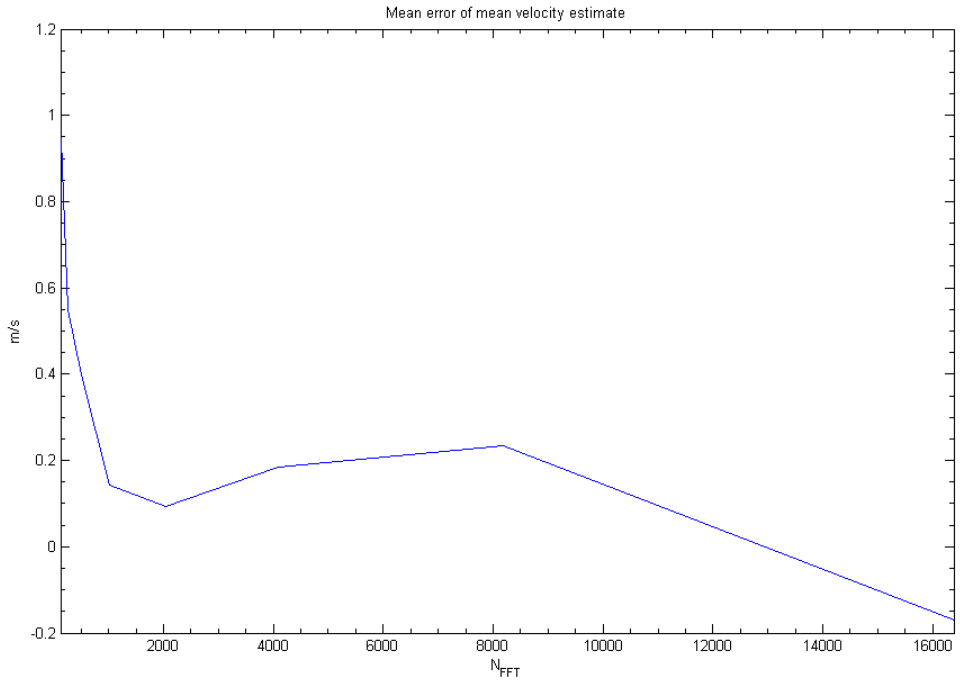


Figure 23. *Mean error of mean velocity estimate using the spectral maxima technique and the SMPRF algorithm vs. $N_{FFT.}$*

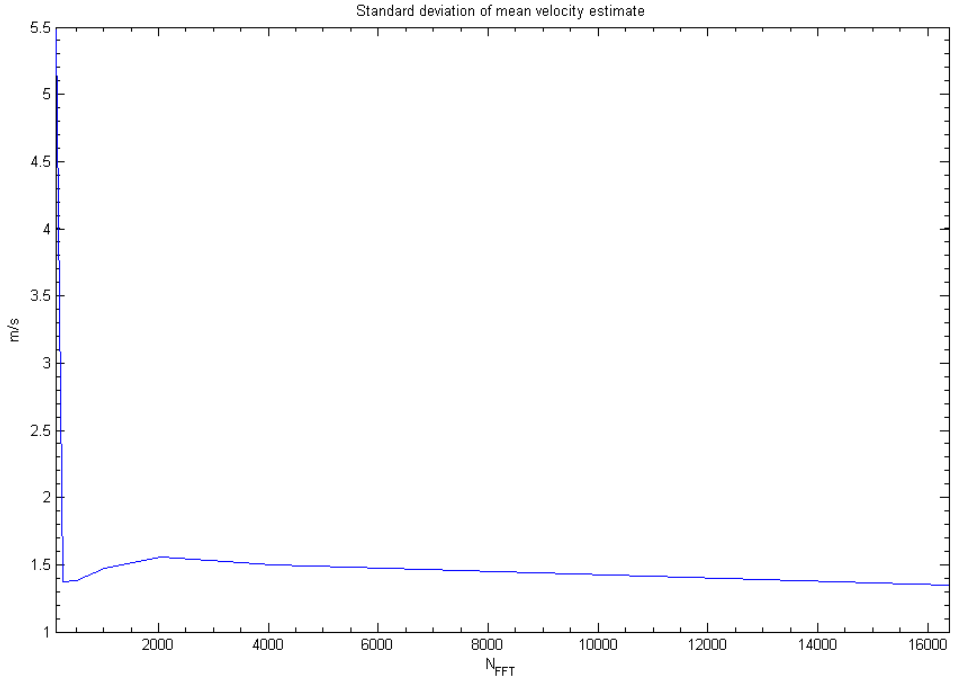


Figure 24. *Standard deviation of mean velocity estimate using the spectral maxima technique and the SMPRF algorithm vs. $N_{FFT.}$*

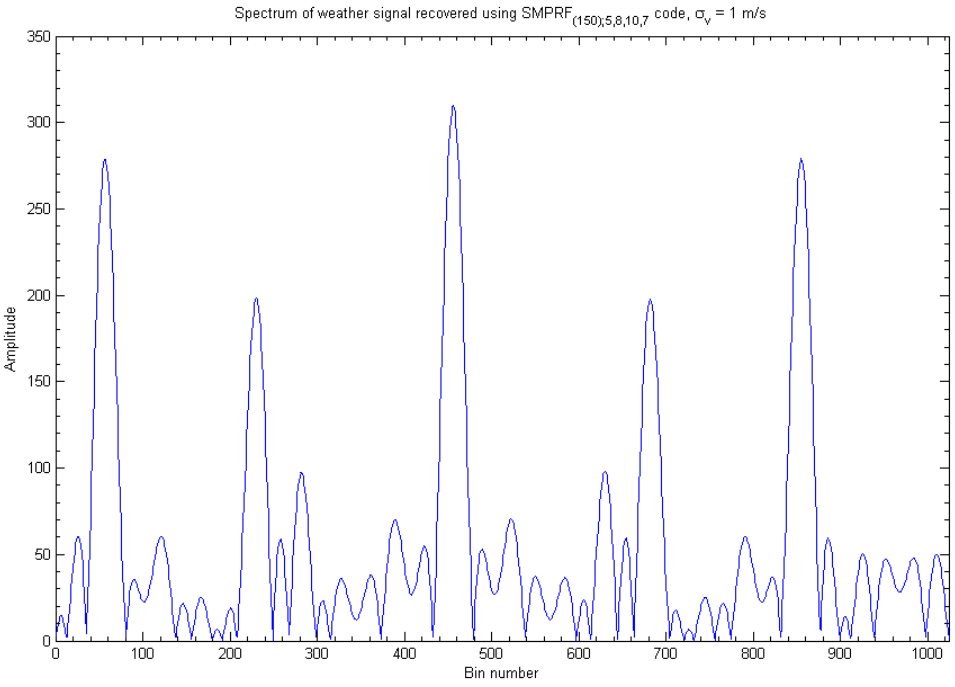


Figure 25. *Spectrum of weather signal recovered using $SMPRF_{(150);5,\ 8,\ 10,\ 7}$ code, $\sigma_v$ = 1 m/s.*

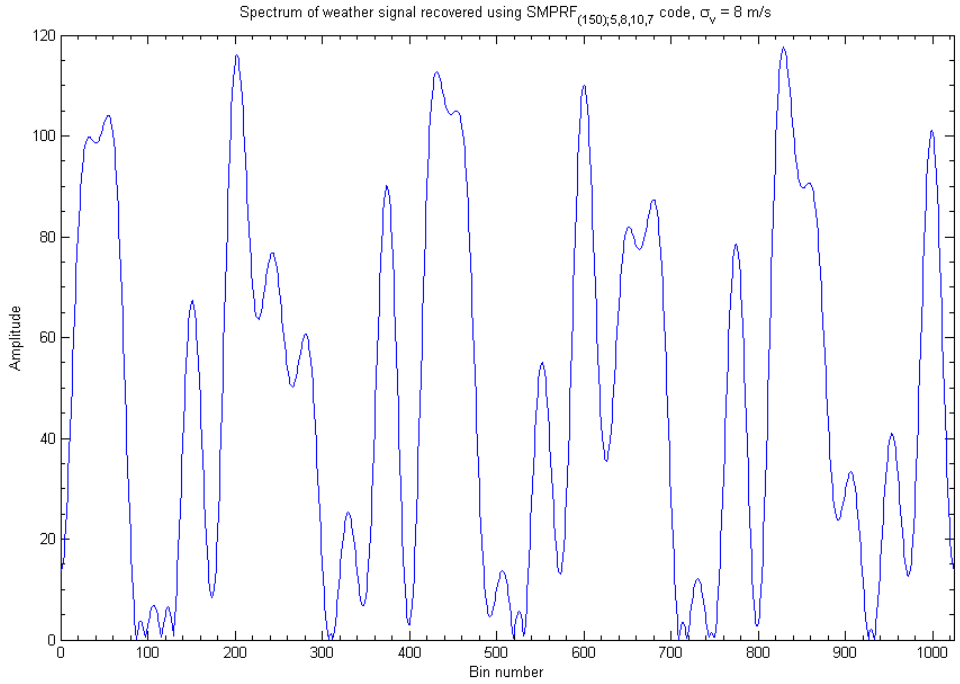


Figure 26. *Spectrum of weather signal recovered using SMPRF$_{(150);5,\ 8,\ 10,\ 7}$ code, $\sigma_v$ = 8 m/s.*

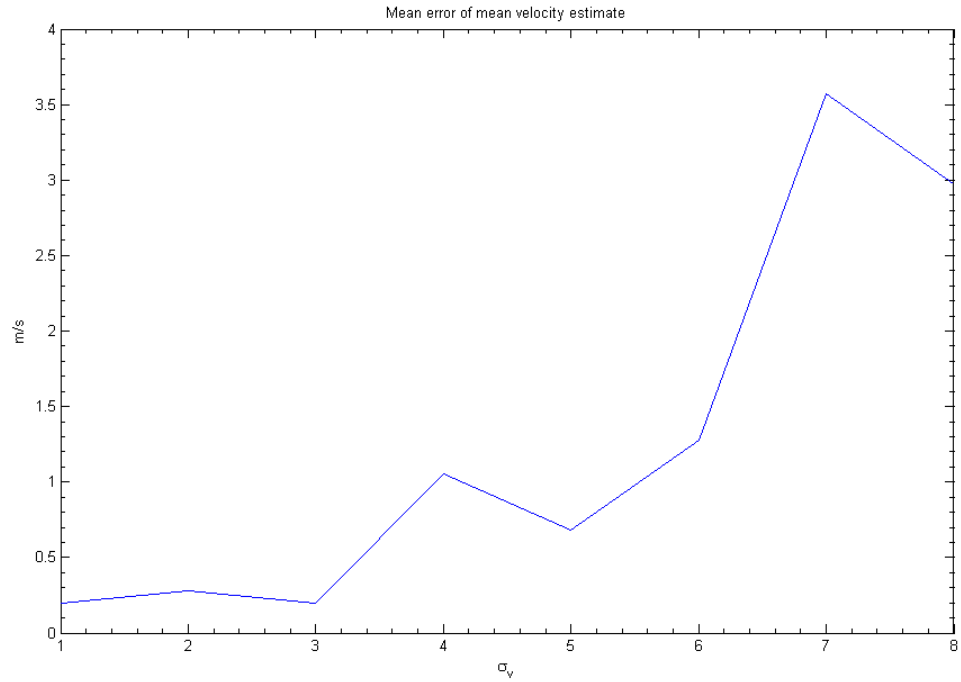


Figure 27. *Mean error of mean velocity estimate using the spectral maxima technique and the SMPRF algorithm vs. $\sigma_{v.}$*

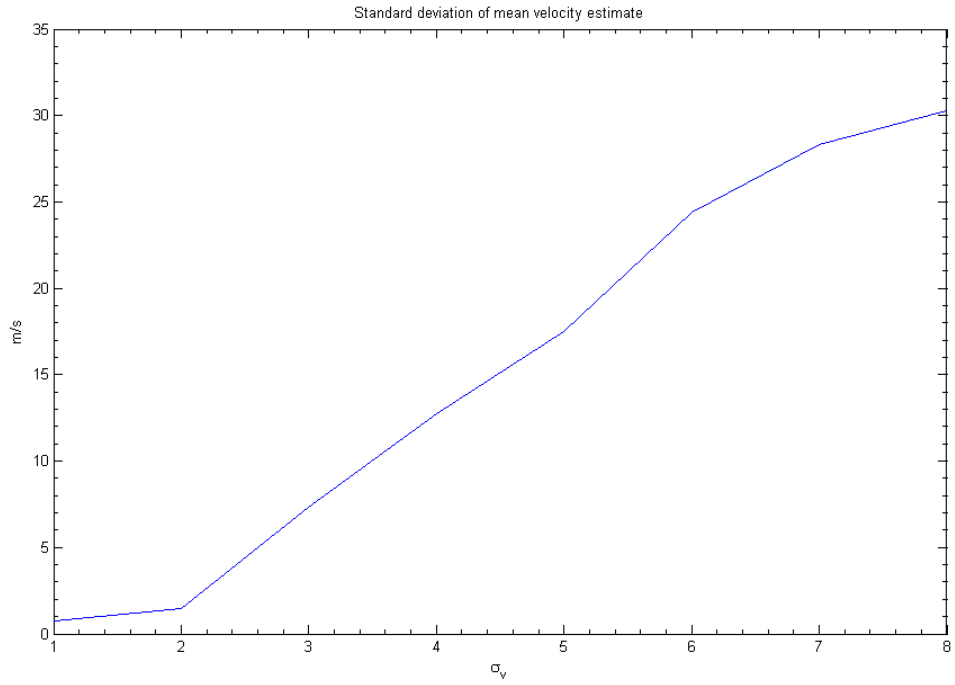


Figure 28. *Standard deviation of mean velocity estimate using the spectral maxima technique and the SMPRF algorithm vs.* $\sigma_{v.}$

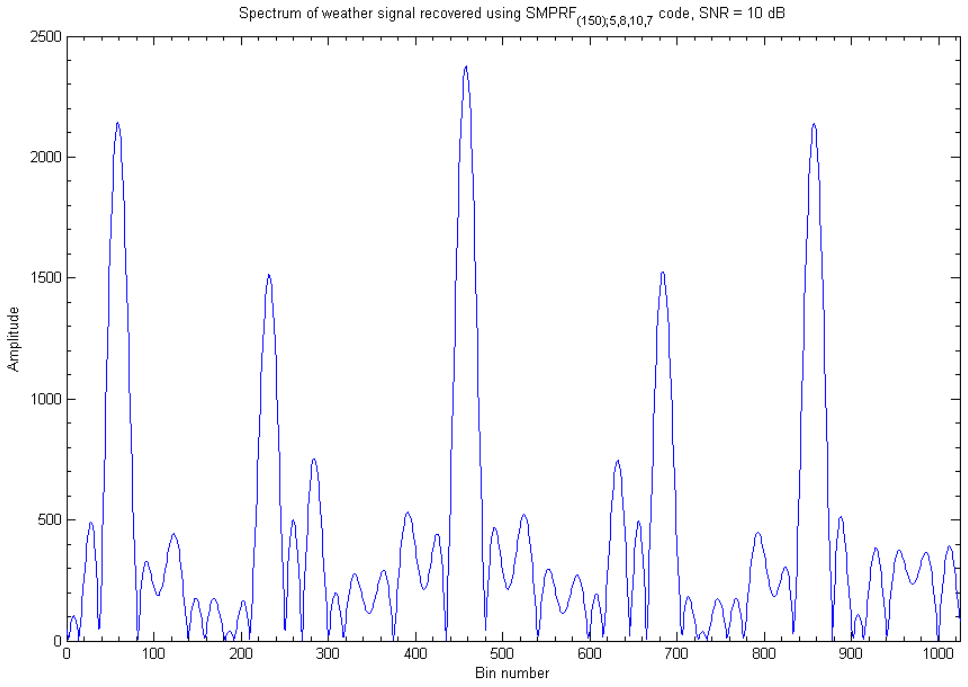


Figure 29. *Spectrum of weather signal recovered using* $SMPRF_{(150);5,\ 8,\ 10,\ 7}$ *code, SNR = 10 dB.*

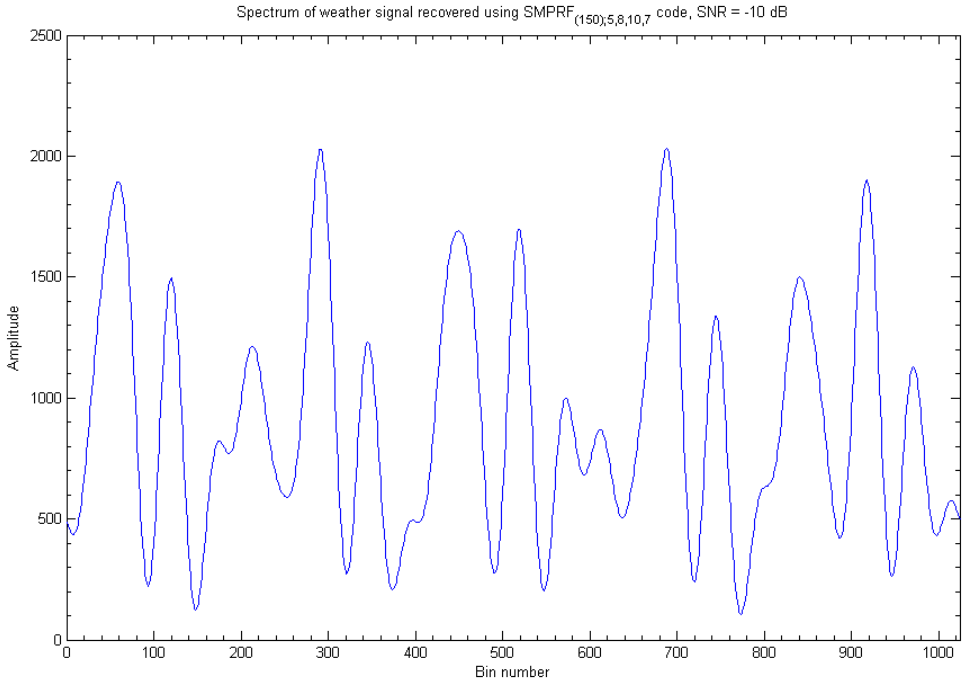


Figure 30. *Spectrum of weather signal recovered using SMPRF$_{(150);5,\ 8,\ 10,\ 7}$ code, SNR = -10 dB.*

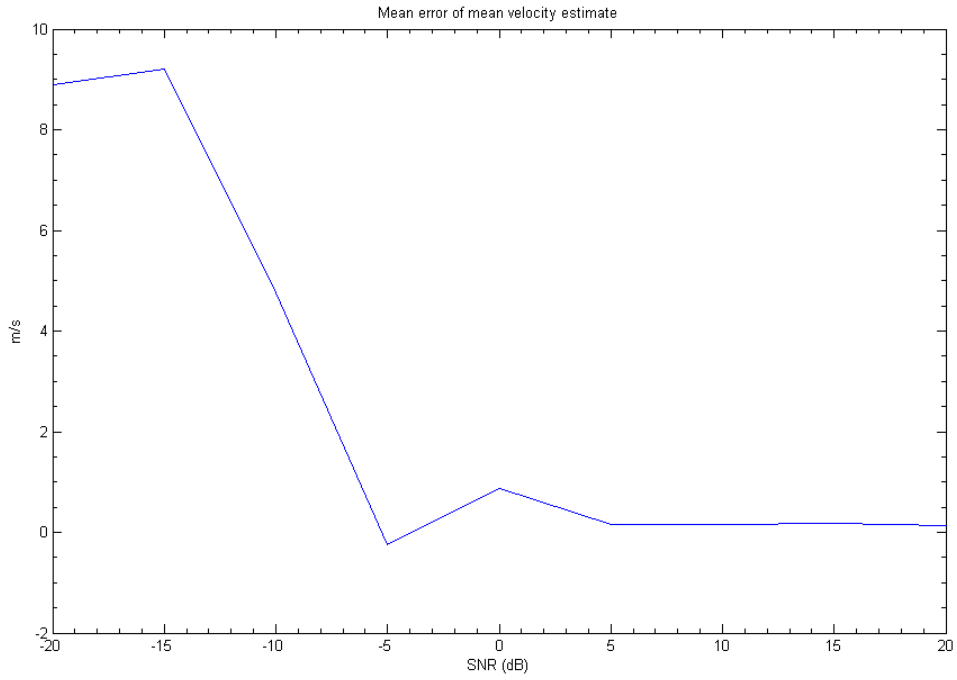


Figure 31. *Mean error of mean velocity estimate using the spectral maxima technique and the SMPRF algorithm vs. SNR.*

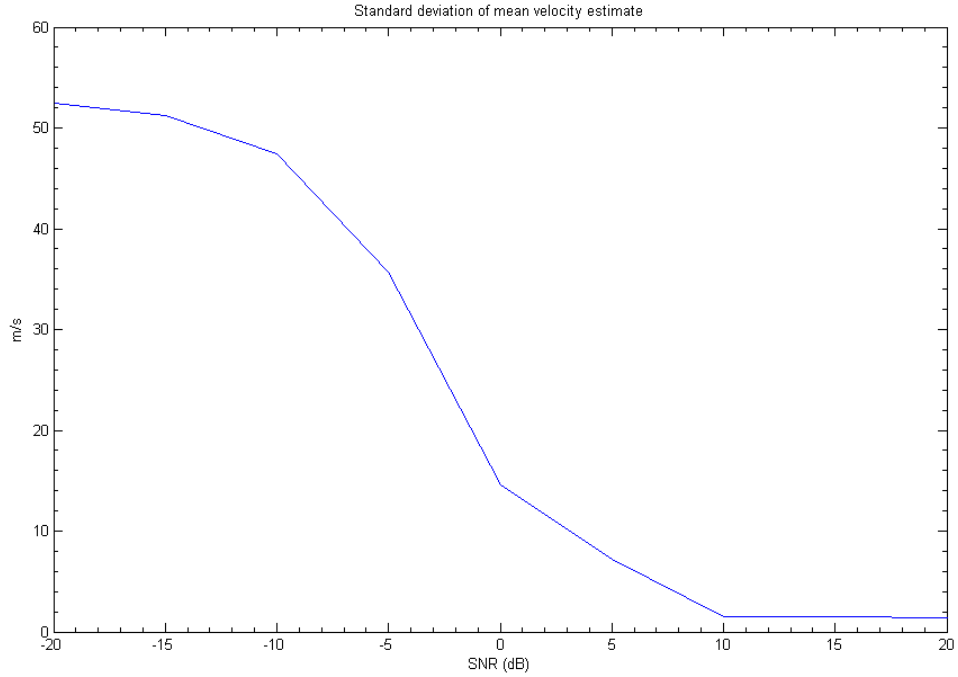


Figure 32. *Standard deviation of mean velocity estimate using the spectral maxima technique and the SMPRF algorithm vs. SNR.*

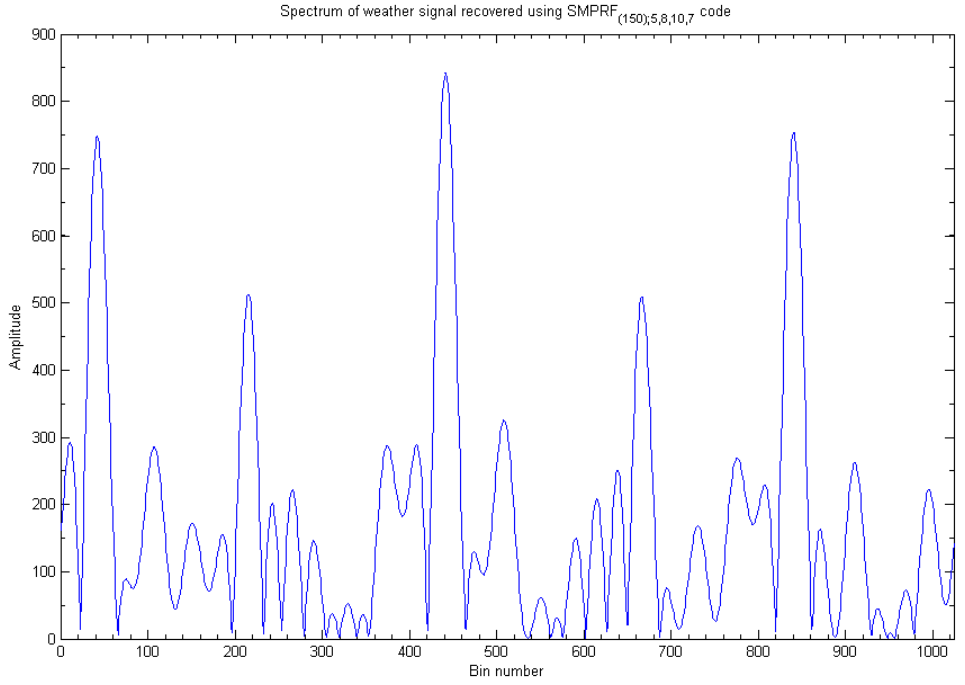


Figure 33. *Spectrum of weather signal recovered using SMPRF$_{(150);5,\ 8,\ 10,\ 7}$ code, lag zero = 0.*

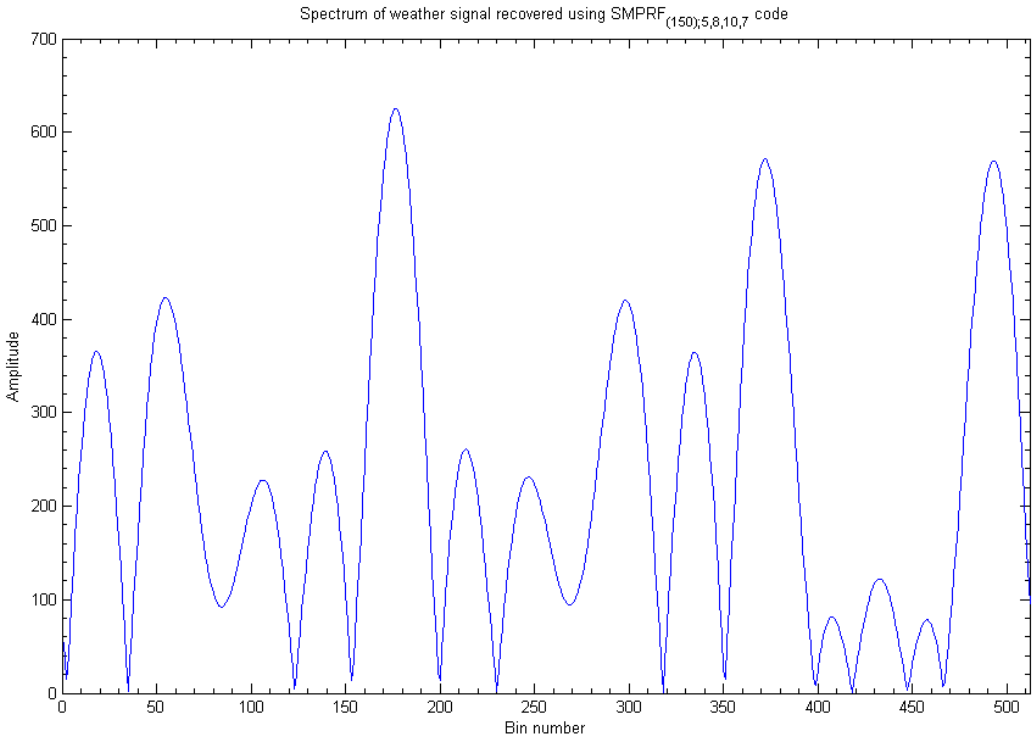


Figure 34. *Spectrum of weather signal recovered using SMPRF$_{(150);5,\ 8,\ 10,\ 7}$ code, using lags 0, 5, and 8.*